



# A double-zero bifurcation in a Lorenz-like system

Antonio Algaba ·  
M. Cinta Domínguez-Moreno ·  
Manuel Merino ·  
Alejandro J. Rodríguez-Luis

Received: 12 June 2023 / Accepted: 18 November 2023 / Published online: 17 December 2023  
© The Author(s) 2023

**Abstract** The Lorenz system presents a double-zero bifurcation (a double-zero eigenvalue with geometric multiplicity two). However, its study by means of standard techniques is not possible because it occurs for a non-isolated equilibrium. To circumvent this difficulty, we add in the third equation a new term,  $Dz^2$ . In this Lorenz-like system, the analysis of the double-zero bifurcation of the equilibrium at the origin guarantees, for certain values of the parameters, the existence of a heteroclinic cycle between the two equilibria located on the  $z$ -axis. The numerical continuation in parameter space of the locus of heteroclinic connections allows to detect various degeneracies of codimension two and three, some of which have not been previously studied in the literature. These bifurcations are organizing centers of the complicated dynamics exhibited by this system. Furthermore, studying how the bifurcation sets

evolve when  $D$  tends to zero, we are able to explain, in the Lorenz system, the origin of several global connections which are related to T-point heteroclinic loops.

**Keywords** Lorenz-like system · Double-zero bifurcation · Global connections · Lorenz system

## 1 Introduction

Lorenz system, since its introduction 60 years ago [1], has become an icon in the world of dynamical systems. Although it was derived from a simplified model of convection in the atmosphere, this system appears in the study of a wide variety of problems (see, for instance, [2–10]). In spite of the hundreds of papers devoted to studying the complex dynamics that it exhibits (see, for example, [11–22] and references therein) the origin of many of its intricate behaviors is still a long way off.

When a specific system is studied, the combination of analytical and numerical methods is usually useful to shed light on concrete aspects of its dynamics, in some region of the parameter space. For example, the application of this strategy to a 3D modified van der Pol–Duffing oscillator, starting with the study of local bifurcations of equilibria, provides very interesting information about its behavior (see, for instance, [23–29] and references therein). Regarding global bifurcations, from the pioneering works of Shilnikov it is well known that they can be at the origin of extremely complicated dynamical behavior (see [30–32] and ref-

---

A. Algaba · M. C. Domínguez-Moreno · M. Merino  
Departamento de Ciencias Integradas, Centro Estudios Avanzados en Física, Matemática y Comp., Universidad de Huelva, 21071 Huelva, Spain  
e-mail: algaba@uhu.es

M. C. Domínguez-Moreno  
e-mail: mcinta.dominguez@dmate.uhu.es

M. Merino  
e-mail: merino@uhu.es

A. J. Rodríguez-Luis (✉)  
Departamento de Matemática Aplicada II, E.T.S. Ingenieros, Universidad de Sevilla, Camino de los Descubrimientos s/n, 41092 Sevilla, Spain  
e-mail: ajrluis@us.es

ferences therein; an excellent survey appears in [30] detailing the important contributions of Shilnikov). A simple analytical way to detect global connections is from a Takens–Bogdanov bifurcation (the linearization matrix has a double-zero eigenvalue with geometric multiplicity one) (see, for example, [33–44] and references therein). If the double-zero eigenvalue has geometric multiplicity two (the so-called double-zero bifurcation), a heteroclinic connection may also appear [45, 46].

In the case of the Lorenz system, some local bifurcations can be studied by standard techniques (analysis of the linearization around an isolated equilibrium, computation of the reduced system on the center manifold, study of the unfolding of the normal form), as the Hopf and Takens–Bogdanov bifurcations [16, 47–49]. However, other singularities (double-zero, Hopf-pitchfork and triple-zero) are exhibited by non-isolated equilibria, which makes their study more difficult [50].

To avoid this problem, we are going to introduce a Lorenz-like system, as simple as possible, that presents a double-zero bifurcation in an isolated equilibrium. Specifically, we will add a single term,  $Dz^2$ , to the third equation of the Lorenz system. In this way, after analyzing this Lorenz-like system, we will obtain valuable information for the Lorenz system by making  $D$  tend to zero (see Fig. 12). Specifically, we will explain how a degenerate heteroclinic connection organizes a family of infinitely many homoclinic orbits previously found in the literature [51, Fig. 6], [52, Fig. 8(B)], [17, Fig. 3], whose origin was unknown. This family is related to a kind of heteroclinic loop called T-point [11, 32, 53–58]. Note that the idea of studying a degenerate heteroclinic cycle in the Lorenz system by introducing new perturbation parameters was already used in Ref. [59].

This paper is organized as follows. In Sect. 2, we introduce the new Lorenz-like system. Section 3 is devoted to the analytical study of the double-zero bifurcation undergone by its equilibrium at the origin (the results obtained are summarized in Theorem 1). The most important outcome is that, in a region of parameter space, the existence of a heteroclinic connection is guaranteed. A detailed numerical analysis, the core of this paper, appears in Sect. 4. The continuation of the heteroclinic orbit emerged from the double-zero bifurcation allows to detect several global bifurcations (homoclinic and heteroclinic connections) of codimension two and three (see Fig. 7) which act as important organizing centers of the dynamics. As far as we

know, the theoretical analysis of three of these degenerate global connections has not been performed so far in the literature. Moreover, we find that the curve of heteroclinic connections accumulates on a line segment of saddle-node bifurcations of periodic orbits (see Fig. 3d). Unlike similar cases known in the literature, this heteroclinic orbit accumulates on a non-hyperbolic periodic orbit. This is because the heteroclinic connection exists on the other side of the saddle-node curve, that is, in the zone where the periodic orbits do not exist. On the other hand, studying how the bifurcation sets evolve when  $D$  tends to zero, we are able to explain, in the Lorenz system, the origin of an infinite sequence of global connections which are related to T-points (see Fig. 12). In this scenario, the three new degenerate global connections mentioned above play a key role. Finally, some conclusions are included in Sect. 5.

## 2 A Lorenz-like system

The Lorenz system is given by (see [1, 60])

$$\begin{aligned}\dot{x} &= \sigma(y - x), \\ \dot{y} &= \rho x - y - xz, \\ \dot{z} &= -bz + xy,\end{aligned}\tag{1}$$

where  $\sigma$ ,  $\rho$  and  $b$  are real parameters. The equilibria are the origin  $(0, 0, 0)$  and a pair of symmetric non-trivial equilibria  $(\pm\sqrt{b(\rho - 1)}, \pm\sqrt{b(\rho - 1)}, \rho - 1)$  when  $b(\rho - 1) > 0$ . The Lorenz equations are invariant under the change  $(x, y, z) \rightarrow (-x, -y, z)$ , which implies that the  $z$ -axis is invariant (and, therefore, there is a heteroclinic connection between the origin and the equilibria at infinity corresponding to this axis).

The characteristic polynomial of its linearization matrix at the origin is given by  $p = \lambda^3 + p_1\lambda^2 + p_2\lambda + p_3$ , with

$$\begin{aligned}p_1 &= b + 1 + \sigma, & p_2 &= \sigma(1 + b - \rho) + b, \\ p_3 &= -b\sigma(\rho - 1).\end{aligned}$$

The origin exhibits a triple-zero bifurcation when  $\sigma = -1$ ,  $\rho = 1$  and  $b = 0$ . In the  $(\rho, b, \sigma)$ -parameter space, three curves of codimension-two bifurcations emerge from this point corresponding to Takens–Bogdanov (when  $\sigma = -1$ ,  $\rho = 1$  and  $b \neq 0$ ), Hopf-pitchfork (if  $\sigma = -1$ ,  $b = 0$  and  $\rho > 1$ ) and double-zero (for  $b = 0$ ,  $\rho = 1$  and  $\sigma \neq -1$ ) singularities of the origin.

Specifically, when the double-zero bifurcation occurs, the linearization matrix has the eigenvalues  $\lambda_1 = \lambda_2 =$

0,  $\lambda_3 = -\sigma - 1$ . But, for these parameter values, the analysis of the origin cannot be performed because it is not an isolated equilibrium. Also, the corresponding normal form is degenerate (all coefficients of  $z^k$  are null). To avoid this, we introduce a new nonlinear term in the third equation,

$$\begin{aligned} \dot{x} &= \sigma(y - x), \\ \dot{y} &= \rho x - y - xz, \\ \dot{z} &= -bz + xy + Dz^2, \end{aligned} \tag{2}$$

where  $D \in \mathbb{R}$ , so that the Lorenz system (1) is embedded in this one. As we will see in Sect. 4, the use of numerical continuation methods will allow us, reaching  $D = 0$ , to obtain valuable information on the Lorenz system.

From now on, in our theoretical analysis we will assume that  $D \neq 0$ . Thus, system (2) can have up to four equilibria, namely

$$E_1 = (0, 0, 0), \quad E_2 = \left(0, 0, \frac{b}{D}\right),$$

$$E_{3,4} = \left(\pm\sqrt{M}, \pm\sqrt{M}, \rho - 1\right),$$

$$\text{with } M = b(\rho - 1) - D(\rho - 1)^2.$$

Observe that  $E_2$  exists if  $D \neq 0$  and  $E_{3,4}$  when  $M > 0$ . Note that, as in the Lorenz system, system (2) is also invariant to the change  $(x, y, z) \rightarrow (-x, -y, z)$ . In this way, the equilibria  $E_1$  and  $E_2$  are always connected by a heteroclinic orbit located on the  $z$ -axis.

The origin  $E_1$  exhibits the following local bifurcations (when  $D \neq 0$ ):

- (i) A pitchfork bifurcation when  $\rho = 1, \sigma \neq -1, b \neq 0$ .
- (ii) A transcritical bifurcation of equilibria, involving  $E_1$  and  $E_2$ , when  $b = 0, \rho \neq 1, \sigma \neq -1$ .
- (iii) A Hopf bifurcation if  $\sigma = -1, \rho > 1, b \neq 0$ .
- (iv) A Takens–Bogdanov bifurcation (a double-zero eigenvalue with geometric multiplicity one) when  $\rho = 1, \sigma = -1, b \neq 0$ .
- (v) A double-zero bifurcation (a double-zero eigenvalue with geometric multiplicity two) for  $\rho = 1, b = 0, \sigma \neq -1$ . In this work, we will analyze this bifurcation.
- (vi) A Hopf-transcritical bifurcation when  $\sigma = -1, b = 0, \rho > 1$ .
- (vii) A degenerate triple-zero bifurcation appears when  $b = 0, \rho = 1, \sigma = -1$ .

Remark that the linearization matrix at the origin is the same for systems (1) and (2). The only bifurcation of the origin that appears in system (2) and not in

the Lorenz system is the transcritical bifurcation (ii). This causes system (2) to undergo a Hopf-transcritical bifurcation instead of a Hopf-pitchfork as in the Lorenz system.

As can be straightforwardly verified, when  $D \neq 0$ , system (2) is symmetric to the change

$$\begin{aligned} (x, y, z, t, \sigma, \rho, b, D) \\ \rightarrow \left(x, y, z - \frac{b}{D}, t, \sigma, \rho - \frac{b}{D}, -b, D\right). \end{aligned} \tag{3}$$

Consequently, all the results obtained for  $E_1$  can be easily translated for  $E_2$ .

### 3 A double-zero bifurcation at the origin

In this section we analyze the double-zero bifurcation undergone by the origin,  $E_1$ . Since this degeneracy occurs when  $\rho = 1, b = 0, \sigma \neq -1, D \neq 0$ , our local study is valid for  $\rho$  and  $b$  close to one and zero, respectively.

The bifurcations that appear in system (2) as a consequence of the double-zero singularity are summarized in the following theorem, whose proof is the core of this section. We will focus on the most interesting case, which occurs when limit cycles appear from a Hopf bifurcation. These periodic orbits disappear in a heteroclinic connection. The corresponding bifurcation sets are drawn in Fig. 1.

**Theorem 1** *The equilibrium  $E_1$  of system (2) undergoes a double-zero bifurcation  $\mathbf{DZ}$  if  $\rho = 1, b = 0, \sigma \neq -1, D \neq 0$ . In a vicinity of this singularity, there are only limit cycles when  $D > 0$  and  $\sigma \in (-\infty, -1) \cup (0, +\infty)$ . In this situation, the following bifurcations appear (see Fig. 1):*

1. A transcritical bifurcation  $\mathbf{T}$ , when  $b = 0$ . It involves the equilibria  $E_1$  and  $E_2$ .
2. Two pitchfork bifurcations,  $\mathbf{P}^1$  for  $\rho = 1$  (concerning  $E_1$  and  $E_{3,4}$ ) and  $\mathbf{P}^2$  when  $b = D(\rho - 1) + \mathcal{O}(\rho^2)$  (involving  $E_2$  and  $E_{3,4}$ ).
3. A Hopf bifurcation  $\mathbf{h}$  of the equilibria  $E_{3,4}$ , when  $b = 2D(\rho - 1), \sigma \neq 1/3$ . This bifurcation is supercritical if  $\sigma > 1/3$ , whereas it is subcritical when  $\sigma < 1/3$ .
4. A heteroclinic cycle connecting  $E_1$  and  $E_2$ , for

$$\begin{aligned} \rho - 1 &= \frac{1}{2D} b + \frac{\sigma(3\sigma - 1)}{8D^2(\sigma + 1)^2(3\sigma + 2D(\sigma + 1))} \\ &\times b^2 + \mathcal{O}(b^3), \end{aligned} \tag{4}$$

when  $\sigma \neq 1/3$ . The global connection is attractive if  $\sigma > 1/3$  and repulsive when  $\sigma < 1/3$ . The loop is formed by two heteroclinic connections: one is placed on the invariant  $z$ -axis (which exists for any value of the parameters and is therefore of zero codimension) and the other one is placed outside this axis (it is structurally unstable).

When the conditions  $D > 0$  and  $\sigma \in (-\infty, -1) \cup (0, +\infty)$  are not fulfilled, only local bifurcations of equilibria (transcritical and pitchfork) are present.

In the analysis of the double-zero bifurcation undergone by  $E_1$  in system (2) (this codimension-two bifurcation occurs when  $\rho = 1, b = 0, \sigma \neq -1, D \neq 0$ ), we first perform the change

$$x = Y - \sigma Z, \quad y = Y + Z, \quad z = X,$$

which converts system (2), for  $b \approx 0$  and  $\rho \approx 1$ , to

$$\begin{aligned} \dot{X} &= -bX + (1 - \sigma)YZ + DX^2 + Y^2 - \sigma Z^2, \\ \dot{Y} &= \sigma^2(1 - \rho)\Delta Z + \sigma(\rho - 1)\Delta Y \\ &\quad - \sigma\Delta XY + \sigma^2\Delta XZ, \\ \dot{Z} &= (\rho - 1)\Delta Y - (1 + \sigma(\sigma + \rho)\Delta)Z \\ &\quad - \Delta XY + \sigma\Delta XZ, \end{aligned} \tag{5}$$

with  $\Delta = \frac{1}{\sigma + 1}, \sigma \neq -1$ . Next, considering the center manifold to second order,  $Z = -\Delta^2 XY + \dots$ , we obtain the reduced system

$$\begin{aligned} \dot{X} &= -bX + DX^2 + Y^2 + \dots, \\ \dot{Y} &= \sigma(\rho - 1)\Delta Y + \sigma\Delta(-1 + (\rho - 1)\sigma\Delta^2) \\ &\quad \times XY + \dots \end{aligned} \tag{6}$$

If we truncate this system to second order, the change  $x = Y, y = X$  leads to

$$\begin{aligned} \dot{x} &= \sigma(\rho - 1)\Delta x + \sigma\Delta(-1 + (\rho - 1)\sigma\Delta^2)xy, \\ \dot{y} &= -by + x^2 + Dy^2. \end{aligned} \tag{7}$$

Now, by means of the change

$$x \rightarrow \frac{1}{\sqrt{|D|}}x, \quad y \rightarrow \frac{-1}{D}y + \frac{b}{2D}, \quad D \neq 0,$$

we obtain

$$\begin{aligned} \dot{x} &= \mu_1 x + axy, \\ \dot{y} &= \mu_2 - \text{sgn}(D)x^2 - y^2, \end{aligned} \tag{8}$$

with

$$\begin{aligned} \mu_1 &= \frac{\sigma\Delta}{2D}(2D(\rho - 1) - b + b(\rho - 1)\sigma\Delta^2), \\ \mu_2 &= \frac{b^2}{4}, \quad a = \frac{\sigma\Delta}{D}(1 + (1 - \rho)\sigma\Delta^2). \end{aligned} \tag{9}$$

Due to its importance in determining the behavior of the system (8), we need to study the sign of  $a$  in the vicinity of  $\rho = 1$  and  $b = 0$ . If  $D > 0$  and  $\sigma \in (-\infty, -1) \cup (0, +\infty)$  or if  $D < 0$  and  $\sigma \in (-1, 0)$ , then  $a > 0$ . Alternatively, when  $D > 0$  and  $\sigma \in (-1, 0)$  or when  $D < 0$  and  $\sigma \in (-\infty, -1) \cup (0, +\infty)$ , we have  $a < 0$ .

System (8) can be analyzed using the study of the Hopf-saddle-node bifurcation carried out in [33, Sect. 4]. Thus, comparing system (8) with [33, Eq. (7.4.9)], we can obtain the bifurcations exhibited by (8). Consequently, we deduce that system (8) is in case III [33, Sect. 4] when  $D > 0$  and  $\sigma \in (-\infty, -1) \cup (0, +\infty)$ . It is in cases IIa-IIb, when  $D < 0$  and  $\sigma \in (-\infty, -1) \cup (0, +\infty)$ . However, as  $\mu_2 = b^2/4 > 0$ , there is no Hopf bifurcation (because, in cases IIa-IIb, it only exists when  $\mu_2 < 0$ ) and only transcritical and pitchfork bifurcations of equilibria appear. Note that the trivial cases I and IV (IVa-IVb), where only equilibria exist (as there are no periodic orbits, there are no global connections either), appear when  $D < 0$  and  $\sigma \in (-1, 0)$  and when  $D > 0$  and  $\sigma \in (-1, 0)$ , respectively.

In what follows we will focus on the case where the most interesting dynamics appears, that is, when there are periodic orbits (if  $D > 0$  and  $\sigma \in (-\infty, -1) \cup (0, +\infty)$ ). Thus, system (8) can have up to four equilibria,

$$\begin{aligned} &\left(0, \pm \frac{b}{2}\right), \\ &\left(\pm \sqrt{N + \mathcal{O}(|b, \rho - 1|^3)}, -D(\rho - 1) + \frac{b}{2}\right), \end{aligned}$$

where  $N = D(\rho - 1)(b - D(\rho - 1))$ , which must be positive for these latter equilibria to exist.

Note that  $E_1$  corresponds to the equilibrium  $(0, -b/2)$  and  $E_2$  to  $(0, b/2)$ .

From the study carried out in [33, Sect. 7.4], we can deduce that the following local bifurcations are present (see Fig. 1):

- A transcritical bifurcation **T**, involving  $E_1$  and  $E_2$ , for  $b = 0$ .
- Two pitchfork bifurcations, **P<sup>1</sup>** for  $\rho = 1$  and **P<sup>2</sup>** if  $b = D(\rho - 1) + \mathcal{O}(\rho^2)$ .
- A Hopf bifurcation **h** of the equilibria  $E_{3,4}$  when  $2D(\rho - 1) = b$ .

As explained in [33, Sect. 7.4], the second-order terms included in system (8) allow neither the study of the Hopf bifurcation nor that of the heteroclinic connection. This is because the system is integrable for the

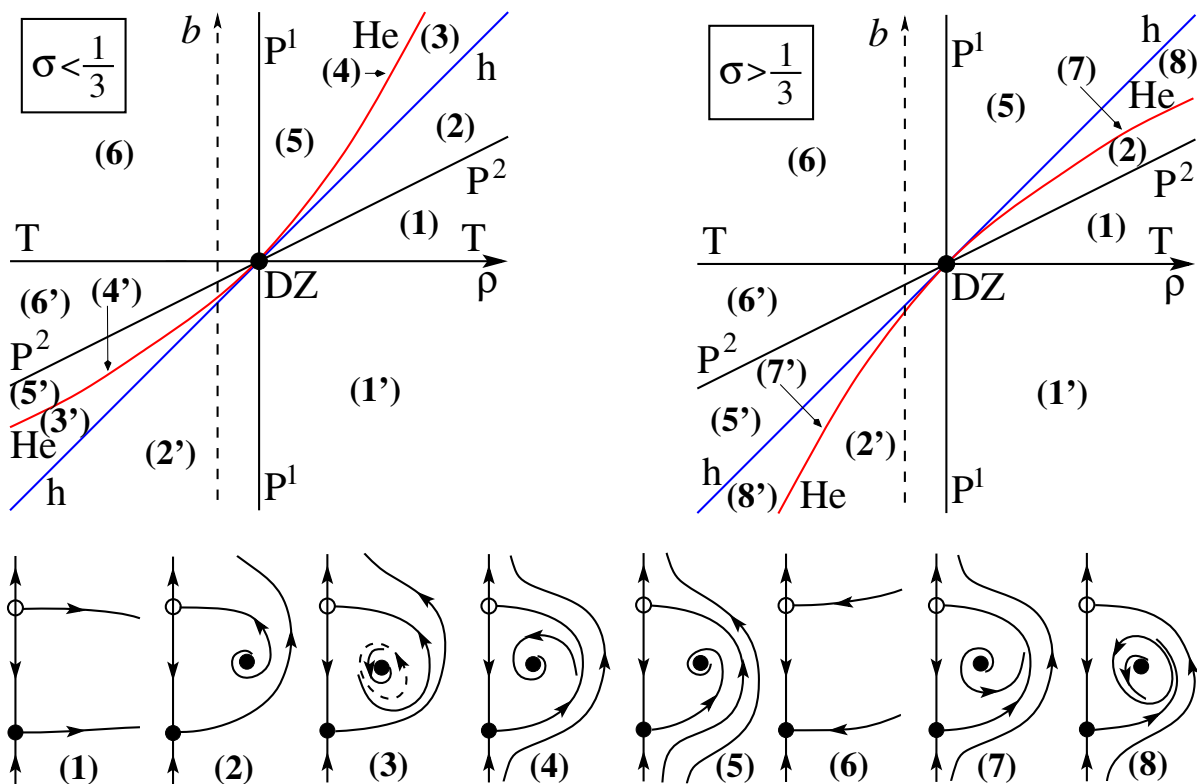


**Fig. 1** Bifurcation set of system (2) in a neighborhood of the double-zero bifurcation **DZ** exhibited by the equilibrium  $E_1$ , for  $D > 0$ , when  $\sigma < 1/3$  (left) and  $\sigma > 1/3$  (right). The curves, according to Theorem 1, correspond to the following bifurcations: **T**, transcritical; **P<sup>1</sup>** and **P<sup>2</sup>**, pitchfork; **h**, Hopf of  $E_{3,4}$  (supercritical when  $\sigma > 1/3$  and subcritical if  $\sigma < 1/3$ ); **He**, heteroclinic loop between  $E_1$  and  $E_2$  (attractive if  $\sigma > 1/3$  and

repulsive when  $\sigma < 1/3$ ). The phase portraits, in the  $(r, \bar{z})$ -plane, are for system (11). On the  $\bar{z}$ -axis, the filled circle represents the equilibrium of (11) that corresponds to equilibrium  $E_1$  in system (2) and the empty circle is used for the equilibrium that corresponds to  $E_2$ . For  $b < 0$ , to obtain the phase portrait in region  $(i')$ , it is enough to interchange the two equilibria on the  $z$ -axis in the phase portrait of region  $(i)$ . (Color figure online)

values of the parameters where the two bifurcations occur: a continuum of periodic orbits bounded by a heteroclinic loop appears (see [33, Fig. 7.4.9] for the easiest case  $a = 2$ ). Therefore, to complete the analysis it is necessary to also include the third-order terms.

Hence, the reduced system of (5) on to the center manifold up to third order,  $Z = \Delta^2 Y(-X + \Delta(D - 2\sigma\Delta)X^2 + \Delta Y^2) + \dots$ , is

$$\begin{aligned} \dot{X} &= -bX + DX^2 + Y^2 + (\sigma - 1)\Delta^2 XY^2, \\ \dot{Y} &= \sigma(\rho - 1)\Delta Y + \sigma\Delta(-1 + (\rho - 1)\sigma\Delta^2)XY \\ &\quad - \sigma^2\Delta^3(\Delta(\rho - 1)(-2\Delta\sigma + D) + 1)X^2Y \\ &\quad - \sigma^2\Delta^4(\rho - 1)Y^3. \end{aligned} \tag{10}$$

The change

$$X = \frac{-1}{D}\bar{z} + \frac{b}{2D}, \quad Y = \frac{2}{\sqrt{2D + (\sigma - 1)\Delta^2 b}}r,$$

transforms (10) into

$$\begin{aligned} \dot{r} &= \tilde{\mu}_1 r + \tilde{a} r \bar{z} + \tilde{c} r^3 + \tilde{d} r \bar{z}^2, \\ \dot{\bar{z}} &= \tilde{\mu}_2 - r^2 - \bar{z}^2 + \tilde{e} r^2 \bar{z}, \end{aligned} \tag{11}$$

where

$$\begin{aligned} \tilde{\mu}_1 &= \sigma\Delta(\rho - 1) - \frac{\sigma\Delta}{2D}b + \frac{\sigma^2\Delta^3}{2D}b(\rho - 1) \\ &\quad - \frac{\sigma^2\Delta^3}{4D^2}b^2 + \mathcal{O}(|b, \rho - 1|^3), \\ \tilde{\mu}_2 &= \frac{b^2}{4} + \mathcal{O}(|b, \rho - 1|^3), \\ \tilde{a} &= \frac{\sigma\Delta}{D} + \mathcal{O}(|b, \rho - 1|), \end{aligned}$$

$$\begin{aligned} \tilde{c} &= \mathcal{O}(|b, \rho - 1|), \quad \tilde{d} = \frac{-\sigma^2 \Delta^3}{D^2} + \mathcal{O}(|b, \rho - 1|), \\ \tilde{e} &= \frac{(\sigma - 1)\Delta^2}{D} + \mathcal{O}(|b, \rho - 1|). \end{aligned}$$

Finally, through the change of coordinates,

$$\begin{aligned} s &= r(1 + g\bar{z}), \quad w = \bar{z} + hr^2 + i\bar{z}^2, \\ \tau &= (1 + j\bar{z})^{-1}t, \end{aligned}$$

where we choose

$$\begin{aligned} g &= \tilde{c} - \tilde{a}h, \quad i = \frac{\tilde{a}\tilde{e} + \tilde{d} - \tilde{c} + 3\tilde{a}h + 2\tilde{a}\tilde{c}}{3\tilde{a}}, \\ j &= \frac{\tilde{a}\tilde{e} - 2\tilde{d} + 2\tilde{c} + 2\tilde{a}\tilde{c}}{3\tilde{a}}, \quad h \in \mathbb{R}, \end{aligned}$$

system (11) becomes

$$\begin{aligned} \frac{ds}{d\tau} &= \hat{\mu}_1 s + \hat{a}sw, \\ \frac{dw}{d\tau} &= \hat{\mu}_2 - s^2 - w^2 + \hat{f}w^3, \end{aligned} \tag{12}$$

where

$$\begin{aligned} \hat{\mu}_1 &= \tilde{\mu}_1 + \mathcal{O}(|b, \rho - 1|^3), \\ \hat{\mu}_2 &= \tilde{\mu}_2 + \mathcal{O}(|b, \rho - 1|^3), \\ \hat{a} &= \tilde{a} + \mathcal{O}(|b, \rho - 1|), \\ \hat{f} &= \frac{\Delta^2(1 - 3\sigma)}{3D} + \mathcal{O}(|b, \rho - 1|). \end{aligned}$$

Thus, in system (12), we can analyze both the Hopf bifurcation and the heteroclinic connection.

Regarding the Hopf bifurcation, a standard analysis provides the first Lyapunov coefficient

$$a_1 = \frac{3\hat{f}}{8\eta}, \quad \text{where} \quad \eta = \frac{\sqrt{2(\hat{\mu}_2 \hat{a}^3 - \hat{\mu}_1^2 \hat{a} - \hat{f} \hat{\mu}_1^3)}}{|\hat{a}|}.$$

If  $a_1 < 0$  the Hopf bifurcation is supercritical, whereas it is subcritical when  $a_1 > 0$ . Consequently, the bifurcation is supercritical if  $\hat{f} < 0$ , i.e. if  $\sigma > 1/3$  and it is subcritical when  $\sigma < 1/3$ . The Hopf bifurcation is degenerate when  $\sigma = 1/3$  (since  $a_1 = 0$ ), this occurs at the point  $(\rho, b, \sigma) = (\rho, 2D(\rho - 1), 1/3)$ .

As far as the heteroclinic connection is concerned, its existence is ensured by Melnikov’s method if  $\hat{f} \neq 0$ , which occurs when  $\sigma \neq 1/3$ . The curve of these global connections is estimated by [36,61,62] (only if  $\hat{a} = 2$  a Hamiltonian case appears [33])

$$\hat{\mu}_1 = \frac{-3\hat{a}^2 \hat{f}}{2(3\hat{a} + 2)} \hat{\mu}_2 + \mathcal{O}(\hat{\mu}_2^2),$$

which according to the original parameters is

$$\rho - 1 = \frac{1}{2D} b + \frac{\sigma \Delta^3 (3\sigma - 1)}{8D^2 (3D\sigma + 2D)} b^2 + \mathcal{O}(b^3)$$

$$\begin{aligned} &= \frac{1}{2D} b + \frac{\sigma(3\sigma - 1)}{8D^2(\sigma + 1)^2(3\sigma + 2D(\sigma + 1))} b^2 \\ &\quad + \mathcal{O}(b^3). \end{aligned}$$

In this way we have already proved all the statements of Theorem 1.

We end this section noting that, when  $\rho = 1, b = 0, \sigma = 1/3, D \neq 0$ , system (2) exhibits a degenerate double-zero bifurcation **DDZ** (because  $\hat{f} = 0$  when  $\sigma = 1/3$ ). Although its local analysis is not complicated, we have not included it here for brevity. To perform it (i.e., to determine the character of the Hopf bifurcation and of the heteroclinic connection), it would be necessary to compute the reduced system of (5) up to fifth order on the center manifold (see similar computations in [45, Sect. 3.1]). From this point **DDZ** in the three-parameter space, two curves **Dh** and **DHe** emerge, corresponding to a degenerate Hopf bifurcation **Dh** and to degenerate heteroclinic connections **DHe**. In the next section we do a global analysis (numerical continuation of the curves that originate at point **DDZ**, whose existence is guaranteed by the local analysis; see Fig. 7). On the other hand, remark that, when  $b = 0$  and  $\sigma = 1/3$ , Lorenz system has an invariant algebraic surface [15].

### 4 Numerical study

Based on the above theoretical analysis, we are going to perform a numerical study with the continuation code AUTO [63]. We will “extend” the bifurcation sets from the vicinity of the double-zero bifurcation **DZ** of the equilibrium  $E_1 = (0, 0, 0)$ , that occurs when  $(\rho, b) = (1, 0)$  and  $\sigma \neq -1, D \neq 0$ . We are going to focus on the case of greatest dynamical richness, that is, when curves of Hopf bifurcation **h** and of heteroclinic connections **He** emerge from the point **DZ** (see Fig. 1). This happens if  $D > 0$  and  $\sigma \in (-\infty, -1) \cup (0, +\infty)$ .

We divide this analysis in two parts. In Sect. 4.1, our objective will be to study the degeneracy of the double-zero bifurcation **DDZ** which, according to the previous analytical study of Sect. 3, appears when  $\sigma = 1/3$ . To do this we will fix  $D = 0.1$  and then we will take slices  $\sigma = constant$  in the  $(\rho, b, \sigma)$ -parameter space, in the vicinity of the point **DDZ** located at  $(1, 0, 1/3)$ . This will allow us to find several degenerate heteroclinic bifurcations, of codimension two and three (see Fig. 7).

In the second part, in Sect. 4.2, we are going to obtain information about the Lorenz system, by making  $D$

tend to zero (see Fig. 12). Specifically, we will explain how some degenerate global connections organize the family of homoclinic orbits previously found in the literature (see [51, Fig. 6], [52, Fig. 8(B)], [17, Fig. 3]), whose origin was unknown.

#### 4.1 Degenerate double-zero

According to the previous analytical study of Sect. 3 there is a degeneracy of the double-zero bifurcation **DZ** when  $\sigma = 1/3$ . So first we fix  $\sigma = 0.3$  and, in order to numerically obtain the bifurcation curves arising from the **DZ** bifurcation point, we are going to draw several bifurcation diagrams (note that, for  $\sigma = 0.3$ , we must obtain the left bifurcation set of Fig. 1).

First, we set  $b = 0.2$  and continue in the parameter  $\rho$  the equilibrium  $E_3$ . It undergoes a Hopf bifurcation that we will denote by **h**, for  $\rho \approx 2.1940452$ . The bifurcation diagram corresponding to the saddle periodic orbit, which arises to the left of **h** for  $b = 0.2$ , appears in Fig. 2a. As can be seen, this periodic orbit does not experience any bifurcation before ending, for  $\rho \approx 2.1907764$ , in a heteroclinic cycle between the equilibria  $E_1 = (0, 0, 0)$  and  $E_2 = (0, 0, 2)$ , which we denote by **He**. This cycle is formed by two heteroclinic connections (see Fig. 2a), the one located on the  $z$ -axis (which exists for any value of the parameters), and the one located outside the  $z$ -axis (which is structurally unstable).

We point out that, in order not to overcomplicate the notation of this work, although a heteroclinic bifurcation (in parameter space) and a heteroclinic cycle (in phase space) are two different objects, we are going to denote them with the same label, **He**. Furthermore, if we have to indicate which equilibrium is involved in a particular bifurcation, we will do so by using a superscript (as we did, for example, with the pitchfork bifurcations **P<sup>1</sup>** and **P<sup>2</sup>** in Theorem 1).

When  $b = 0.3$  (see Fig. 2b), a stable periodic orbit arises from the Hopf bifurcation **h** ( $\rho \approx 2.9069632$ ) to the right. Subsequently, for  $\rho \approx 2.9072735$ , it undergoes a saddle-node bifurcation of periodic orbits **sn** when it collapses with a saddle periodic orbit which finally disappears in a heteroclinic cycle for  $\rho \approx 2.9068041$ . Finally, in Fig. 2c, for  $b = -0.2$ , we show the bifurcation diagram corresponding to the saddle periodic orbit, which arises to the left of **h**. As in the case  $b = 0.2$  this periodic orbit does not experience

any bifurcation before ending in a heteroclinic cycle between  $E_2 = (0, 0, -2)$  and  $E_1 = (0, 0, 0)$ , for  $\rho \approx 0.1907764$ . Its projection onto the  $(x, z)$ -plane also appears in Fig. 2c. We note that the results obtained for  $b = -0.2$  were expected due to the symmetry that system (2) has: when passing through  $b = 0$  the equilibria  $E_1$  and  $E_2$  undergo the transcritical bifurcation **T**, and consequently the above diagram can be easily obtained by applying the change of variables (3).

Now we can numerically compute in the  $(\rho, b)$ -plane the bifurcation curves detected in the diagrams of Fig. 2 for  $\sigma = 0.3$ . Thus, in Fig. 3a we have drawn the three straight lines that intersect at the double-zero bifurcation point **DZ**, namely **P<sup>1</sup>**, pitchfork bifurcation of  $E_1$  for  $\rho = 1$ , **P<sup>2</sup>**, pitchfork bifurcation of  $E_2$  for  $b = 0.1(\rho - 1)$  and **T**, transcritical bifurcation between  $E_1$  and  $E_2$  for  $b = 0$ . We also see the curves **h** and **He** corresponding, respectively, to Hopf bifurcations of the equilibria  $E_{3,4}$  and to heteroclinic connections between the equilibria  $E_1$  and  $E_2$ . In particular, the Hopf bifurcation curve **h** is given by:

$$\begin{aligned}
 & [2D(\rho - 1) - b - \sigma - 1][b(\rho + \sigma) - 2D(\rho - 1)\sigma \\
 & \quad + D(1 - \rho^2)] + 2(b - D(\rho - 1))(\rho - 1)\sigma = 0, \\
 & 2D(\rho - 1) - b - \sigma - 1 \neq 0, \\
 & b(\rho + \sigma) - 2D(\rho - 1)\sigma + D(1 - \rho^2) > 0. \tag{13}
 \end{aligned}$$

Note that when  $D = 0$ , (13) coincides with the expression for the curve of the Hopf bifurcation of the non-trivial equilibria in the Lorenz system [48, Sect. 3.1].

Let us remember that due to the symmetry that system (2) presents, we can easily obtain the third quadrant of the bifurcation set by applying the change of variables (3) to each of the curves of the first quadrant. For this reason, in what follows, we will only focus on the first quadrant.

To analyze some of the degeneracies that may exist on the curve **He** in the first quadrant of the parameter plane  $(\rho, b)$ , we will denote by  $\lambda_1, \lambda_2, \lambda_3$  the eigenvalues of the Jacobian matrix at  $E_1 = (0, 0, 0)$  and  $\lambda_1^*, \lambda_2^*, \lambda_3^*$  the eigenvalues of the Jacobian matrix at  $E_2 = (0, 0, b/D)$ , where

$$\lambda_{1,2} = \frac{-(1 + \sigma) \pm \sqrt{(1 - \sigma)^2 + 4\sigma\rho}}{2}, \quad \lambda_3 = -b,$$

and

$$\begin{aligned}
 \lambda_{1,2}^* &= \frac{-(1 + \sigma) \pm \sqrt{(1 - \sigma)^2 + 4\sigma(\rho - b/D)}}{2}, \\
 \lambda_3^* &= b. \tag{14}
 \end{aligned}$$

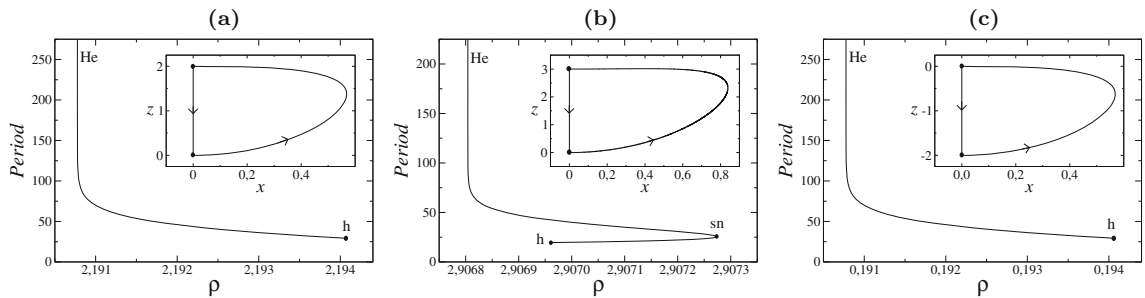


**Fig. 2** For  $\sigma = 0.3$  and  $D = 0.1$ , bifurcation diagram of the asymmetric periodic orbit born in the bifurcation Hopf **h** of the equilibrium  $E_3$  for: **a**  $b = 0.2$ . **b**  $b = 0.3$ . **c**  $b = -0.2$ . In the inset of panels **(a–c)**, projection onto the  $(x, z)$ -plane of the

roclincic cycle **He** connecting the origin  $E_1$  and  $E_2$ , that exist for  $\rho \approx 2.1907764$ ,  $\rho \approx 2.9068041$  and  $\rho \approx 0.1907764$ , respectively

Note that in the first quadrant of the parameter plane  $\lambda_2 < \lambda_3 < 0 < \lambda_1$  and  $Re(\lambda_2^*) \leq Re(\lambda_1^*) < 0 < \lambda_3^*$ . In this case, the saddle quantities are given by  $\delta_1 = \left| \frac{\lambda_3}{\lambda_1} \right|$  and  $\delta_2 = \left| \frac{Re(\lambda_1^*)}{\lambda_3^*} \right|$ . The saddle quantity corresponding to the heteroclinic cycle is given by the product  $\delta_1 \delta_2 \equiv \delta_{12}$  (when  $\delta_{12} = 1$  the heteroclinic cycle is degenerate [33]). Moreover, in a neighborhood of the point **DZ** = (1, 0) in the first quadrant, the eigenvalues of  $E_2$  are real, consequently  $\delta_2 = \left| \frac{\lambda_1^*}{\lambda_3^*} \right|$ . Therefore, the curve where the product  $\delta_1 \delta_2 \equiv \delta_{12} = 1$  satisfies the equation

$$b = \frac{(1 + \sigma)D \left[ -(1 + \sigma) + \sqrt{(1 + \sigma)^2 - 4\sigma(1 - \rho)} \right]}{\sigma} \tag{15}$$

Initially the Hopf bifurcation curve **h** arises from the point **DZ** to the right of the heteroclinic connection curve **He**, being subcritical (see Theorem 1). As can be seen in Fig. 3a, on the curve **h** there is a degeneracy of codimension two at the point **Dh**, that occurs when  $(\rho, b) \approx (2.7093960, 0.2730477)$ , where the first Lyapunov coefficient  $a_1$  vanishes. From this point **Dh** a saddle-node bifurcation curve of periodic orbits **sn** arises (this curve is drawn in the inset of Fig. 3a). It ends in another degeneracy **DHe**, for  $(\rho, b) \approx (3.1169844, 0.3279419)$ , located on the curve of heteroclinic connections **He**, where it is verified that  $\delta_{12} = 1$ . We remark that the curves **h** and **He** intersect at the point  $(\rho, b) \approx (2.925824, 0.302549)$  and they change their relative position (this change can be seen better in Fig. 3c). At the points of the curve **He** between

the degeneracies **DZ** and **DHe**, it is true that  $\delta_{12} < 1$  and, in accordance with the bifurcation diagrams in Fig. 2, a saddle periodic orbit arises from the heteroclinic cycle. Next, on the curve **He** a new degeneracy **DHe<sup>2</sup>** appears for  $(\rho, b) \approx (3.9754280, 0.43837613)$ , where  $\lambda_1^* = \lambda_2^* = -0.65$  and, as a consequence, in the remaining points the equilibrium  $E_2$  changes its configuration, becoming a saddle-focus since both eigenvalues are now complex. Note that we use superscripts to indicate on the curve **He** which of the two equilibria ( $E_1$  or  $E_2$ ) experiences a certain degeneracy. The previous change implies that, in the range of Fig. 3a in the first quadrant, the expression of the curve where  $\delta_{12} = 1$  is now

$$\rho = \frac{3 + 10\sigma + 3\sigma^2}{4\sigma}, \tag{16}$$

instead of Eq. (15). As we can see, this expression does not depend on  $b$ , since now  $\delta_2 = \left| \frac{Re(\lambda_1^*)}{\lambda_3^*} \right|$ . Note that in the range of Fig. 3a, on the curve **h** there is another degenerate point **Dh**, for  $(\rho, b) \approx (4.17986, 0.466067)$ , where  $a_1 = 0$ . As we will see later in Fig. 7, this second **Dh** point is not involved in the degeneracy **DDZ** of the double-zero bifurcation. The fold of the curve **Dh** with respect to  $\sigma$  explains its existence when  $\sigma = 0.3$ .

From our numerical study we deduce that the dynamics around the point **DHe<sup>2</sup>** is very complex (this bifurcation will be considered in more detail in Sect. 4.2). Thus, we conjecture the existence of an infinite sequence of bifurcation curves of various types that emanate from this point: saddle-nodes of asymmetric and symmetric periodic orbits, period-doublings of the asymmetric periodic orbits, symmetry-breakings of

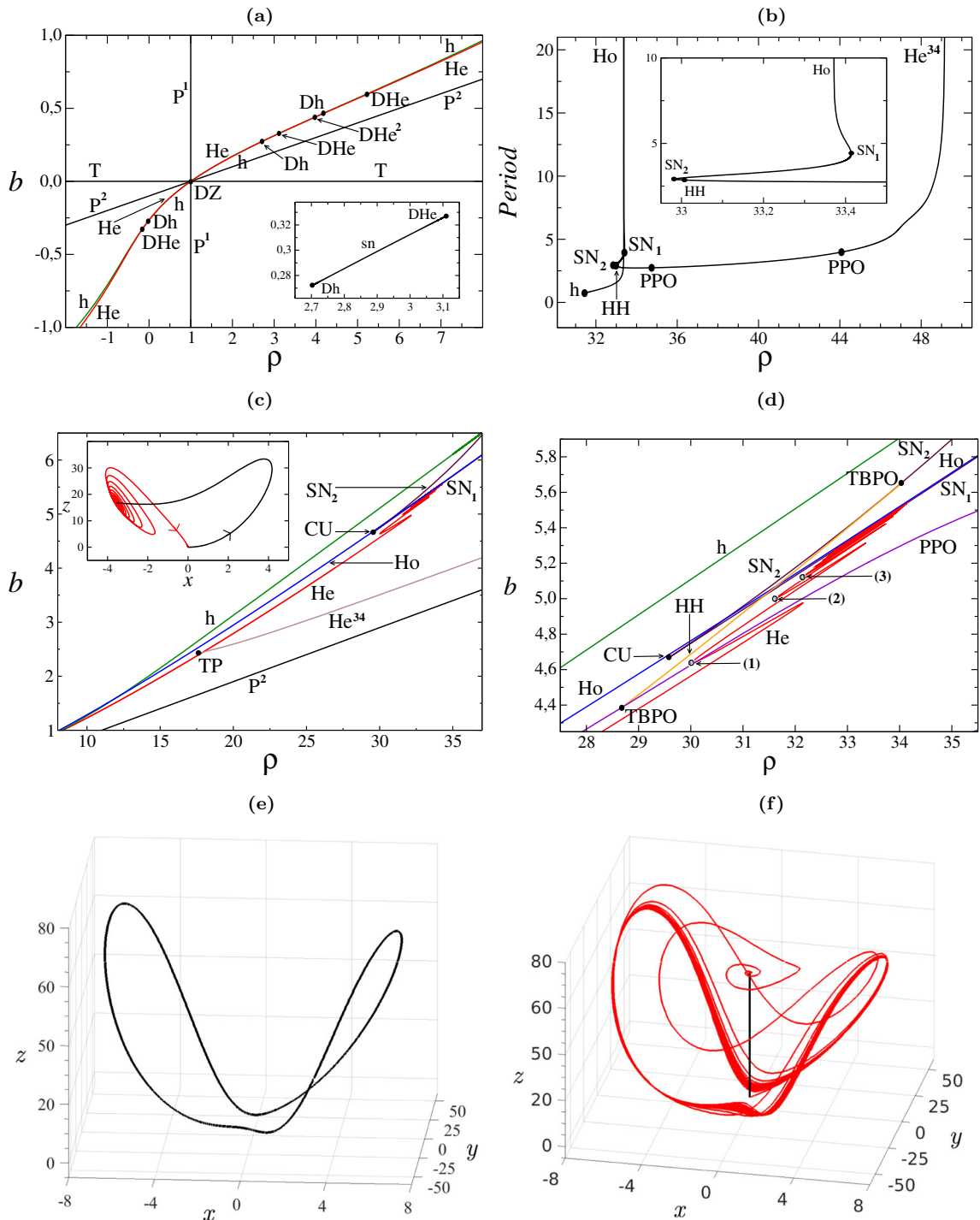


**Fig. 3** For  $\sigma = 0.3$ ,  $D = 0.1$ : **a** Partial bifurcation set in a neighborhood of the double-zero point **DZ**. **b** Bifurcation diagram for  $b = 5.4$ . **c** Partial bifurcation set in the first quadrant, in a range outside the panel (a). The projection on the  $(x, z)$ -plane of the T-point **TP** is drawn in the inset. **d** Zoom of panel c near the accu-

mulation process of **He**. For  $b = 5.4$ : **e** a degenerate symmetric periodic orbit, placed on the curve **SN<sub>1</sub>**, for  $\rho \approx 33.413688$ ; **f** the heteroclinic cycle on **He**, for  $\rho \approx 33.414582$  (the black line corresponds to the connection placed on the invariant  $z$ -axis). (Color figure online)

the symmetric periodic orbits, homoclinic connections of the origin..., which implies the existence of diverse types of attractors in a neighborhood of the origin (see [45, Fig. 8]). In Fig. 3c we have included one of them, **Ho** (blue color), the first curve of the sequence of homoclinic connections of the origin that arise from the point **DHe**<sup>2</sup>. This interesting point that, as far as we know, has not been studied in the literature, will deserve to be analyzed theoretically in the future. In this work we restrict ourselves to studying some of the bifurcations that it organizes in system (2) and that will give us information about the Lorenz system (see Sect. 4.2).

Once we have numerically found all the bifurcation curves whose existence is guaranteed by the analysis of the double-zero degeneracy, we are going to study in more depth the behavior of the heteroclinic curve **He** as we move away from the point **DZ**. For this task we are going to detect new bifurcations by considering the diagram of Fig. 3b, for  $b = 5.4$ . We see that now the pair of asymmetric attractive periodic orbits, that arises from the Hopf bifurcation **h**, ends at a homoclinic connection of the origin, **Ho**. Moreover, the symmetric attractive periodic orbit that also arises from **Ho** ends in a heteroclinic connection between the equilibria  $E_{3,4}$ , **He**<sup>34</sup>. As observed in the bifurcation diagram, the symmetric periodic orbit exhibits several bifurcations, namely: two saddle-node bifurcations, **SN**<sub>1</sub> and **SN**<sub>2</sub>, a torus bifurcation **HH** and two symmetry-breaking bifurcations, **PPO**.

We are now in a position to see that the heteroclinic curve **He** ends in an interesting accumulation process. In Fig. 3c we have drawn a partial bifurcation set, in the first quadrant, at another range of values furthest from **DZ**. In addition to the curves **P**<sup>2</sup>, **h** and **He**, we can see two curves of saddle-node bifurcation of symmetric periodic orbits, **SN**<sub>1</sub> and **SN**<sub>2</sub>. Both curves collapse at the cusp point **CU**, when  $(\rho, b) \approx (29.57655304, 4.6665097)$ . The curve **Ho** (of homoclinic connections of the origin) is located to the left of **SN**<sub>1</sub> in the range of this figure. We observe that the curve **He** experiences a sequence of oscillations, each time closer to each other, which accumulates to the curve **SN**<sub>1</sub>. In this figure we have also included the curve of heteroclinic connections **He**<sup>34</sup> between the equilibria  $E_{3,4}$  (brown color), which arises from the point **TP**, for  $(\rho, b) \approx (17.7017834, 2.4215793)$ , where a heteroclinic cycle, called (principal) T-point, exists. The projection onto the  $(x, z)$ -plane of the T-point **TP** heteroclinic loop is drawn in the inset of

Fig. 3c, where the black line corresponds to the intersection between the one-dimensional manifolds of the equilibria  $E_1$  and  $E_4$  and the red one to the intersection between the two-dimensional manifolds. This codimension-two bifurcation organizes three curves of global connections corresponding to homoclinic orbits of the origin and to homoclinic and heteroclinic orbits of the equilibria  $E_{3,4}$  [11, 17, 32]. We note that the curve **SN**<sub>1</sub> is related to a degeneracy that appears, outside the range of Fig. 3c, on the curve **He**<sup>34</sup>.

In the zoom shown in Fig. 3d, we can observe better that the curve **He** accumulates on a line segment on **SN**<sub>1</sub>. As a consequence, the heteroclinic orbit itself accumulates on the corresponding non-hyperbolic periodic orbit placed on **SN**<sub>1</sub>, as can be seen in Fig. 3e, f when  $b = 5.4$ . We have drawn, respectively, the phase portraits of the degenerate symmetric periodic orbit that exists when  $\rho \approx 33.413688$  on the curve **SN**<sub>1</sub> and of the heteroclinic orbit on the curve **He** for  $\rho \approx 33.414582$  (in this accumulation process, the heteroclinic orbit performs more and more windings around the non-hyperbolic periodic orbit). On the other hand, in Fig. 3d we have also drawn the curves of the other bifurcations present in the diagram of Fig. 3b. Thus, the torus bifurcation **HH** exists between the curves **SN**<sub>2</sub> and **PPO**. The endpoints of **HH** correspond to Takens–Bogdanov bifurcations of periodic orbits **TBPO** (double +1 Floquet multiplier with geometric multiplicity one), also named 1:1 resonances of periodic orbits [64]. Examples of this situation can be found for the Lorenz system in [20, 49]. Although in this work we do not focus on them, it should be noted that the cascades of period-doubling bifurcations, exhibited by the asymmetric periodic orbits emerged from the symmetry-breaking bifurcations **PPO**, give rise to a sequence of Takens–Bogdanov bifurcations of periodic orbits (with double -1 Floquet multiplier), also named 1:2 resonances of periodic orbits. The complex dynamics present in this scenario is illustrated, for instance, in the figures of the works [20, 49].

A similar accumulation process, but relative to a curve of homoclinic connections, has been found in [65] where a curve of homoclinic orbits accumulates on a segment in parameter space while the homoclinic orbit itself approaches a saddle periodic orbit. A theoretical study of this type of behavior has been carried out in [66]. It is interesting to note the following fact. Although in our case there is no saddle periodic orbit in the region where the curve ends up accumulating

over a segment of  $\mathbf{SN}_1$  (the saddle periodic orbit exists in the region between the curves  $\mathbf{SN}_1$  and  $\mathbf{SN}_2$ ), however, the heteroclinic orbit behaves in a similar way to the homoclinic orbit studied in [65,66]. Let us discuss those details.

In the accumulation process of the curve  $\mathbf{He}$ , the maxima and the minima (with respect to  $\rho$ ) converge to separate points on  $\mathbf{SN}_1$  (that limit the accumulation segment of  $\mathbf{He}$ ). To understand the evolution of the heteroclinic orbit (located outside the  $z$ -axis) along the curve  $\mathbf{He}$  we are going to look at how it changes in the first minima, marked as **(1)**, **(2)** and **(3)** in Fig.3d. In Fig.4a, c we have drawn, for  $\sigma = 0.3$ , the projections on the  $(x, z)$ -plane of the heteroclinic orbits labelled **(1)** and **(3)**, placed, respectively, at  $(\rho, b) \approx (30.0154396, 4.6367200)$  and  $(\rho, b) \approx (32.1468879, 5.1240339)$ . Their temporal profiles  $t$ - $z$  appear in Fig.4b, d. As can be seen in these figures (similarly as it occurs in [65, Fig. 10] with the homoclinic orbits), if we start from the heteroclinic orbit **(1)**, to go around each of the non-trivial equilibria  $E_{3,4}$  (black bullets) one more time, we have to go to the point **(3)** of the curve  $\mathbf{He}$ , that is, go through two oscillations on such a curve. We note that the projection onto the  $(x, z)$ -plane of the heteroclinic orbit corresponding to the point **(2)**, placed at  $(\rho, b) \approx (31.6099774, 4.9976719)$ , surrounds equilibrium  $E_3$  twice and equilibrium  $E_4$  only one time.

In [65, Table 1] (inspired by the results of the theoretical analysis carried out in [66]) the authors build a table to check if consecutive maxima (or minima) of the homoclinic curve converge to their limit with a rate given by the stable eigenvalue of the saddle-periodic orbit to which the homoclinic orbit approaches. Their table contains data of the distances  $\text{dist}(i)$  between the  $i$ th and the  $(i - 1)$ st maximum of the homoclinic curve. The numbers  $\text{dist}(i)$  were determined as the Euclidean distances between fold points (LP) detected by AUTO/HomCont during continuation of the homoclinic curve. It seems that the ratios converge (within numerical accuracy) to the stable Floquet multiplier. In our case, as the periodic orbit to which the heteroclinic cycle approaches is non-hyperbolic (it is on the curve  $\mathbf{SN}_1$ ), we want to check if the ratios of the distances converge to the Floquet multiplier 1. We consider the minima (with respect to  $\rho$ ) of Fig.3d, where the point labelled **(1)** is the first minimum ( $i = 1$ ). The results appear in Table 1 and, according to them, it is plausible that the ratios converge to 1.

**Table 1** For  $\sigma = 0.3$  and  $D = 0.1$ , distances  $\text{dist}(i)$  between the  $(i + 1)$ th and the  $i$ th minimum of the curve  $\mathbf{He}$  and their ratios,  $\text{dist}(i)/\text{dist}(i - 1)$

$i$	$\text{dist}(i)$	$\text{dist}(i)/\text{dist}(i - 1)$
1	1.6348813716	
2	0.5515797634	0.3373821324
3	0.2510243729	0.4551007660
4	0.1345820461	0.5361313904
5	0.0803617162	0.5971206302
6	0.0518220796	0.6448602905
10	0.0142412156	0.7614073846
20	0.0022340045	0.8692080074
40	3.2262084789e-04	0.9306352572
60	1.0097576035e-04	0.9526560989
100	2.2851831113e-05	0.9709947053

The point labelled **(1)** in Fig.3d is the first minimum. It seems that the ratio approaches the Floquet multiplier +1 of the non-hyperbolic periodic orbit on which the heteroclinic orbit accumulates

When  $D = 0.1$ , to verify the above and determine the existence of other degeneracies on the curve  $\mathbf{He}$ , we have drawn in Fig.5a, for  $\sigma = 0.3$ , the value of the product  $\delta_{12}$  at the points of the curve  $\mathbf{He}$  in a wider range than that of Fig.3a, namely when  $b \in (0, 2.5]$ . In fact, in this figure it can be observed that, in the neighborhood of the point  $\mathbf{DZ}$ , the product  $\delta_{12} < 1$  for the points of the curve  $\mathbf{He}$ . Subsequently, there is a value (red bullet) where  $\delta_{12} = 1$ , being both saddle-node equilibrium points (this point of the graph corresponds to the lowest point  $\mathbf{DHe}$  of the curve  $\mathbf{He}$  in the first quadrant in Fig.3a). Next, in the zone where  $\delta_{12} > 1$ , the existence of a maximum is observed. This maximum corresponds to the point  $\mathbf{DHe}^2$  in Fig.3a on the curve  $\mathbf{He}$  where a double eigenvalue  $\lambda_1^* = \lambda_2^*$  appears. Finally, the existence of another point (blue bullet) is observed where, being the equilibrium  $E_1$  a real saddle and  $E_2$  a saddle-focus, it is true that  $\delta_{12} = 1$ . This point on the graph corresponds to the upper point  $\mathbf{DHe}$  for  $(\rho, b) \approx (5.225, 0.5951172)$  which appears in Fig.3a. As we will see later, this degeneration is not related to the double-zero degeneracy  $\mathbf{DZ}$  analyzed in this work. In the remaining points, it is observed that  $\delta_{12} < 1$  and its value decreases as  $b$  increases.

In Fig.5b we have made a similar graph for  $\sigma = 0.2$ , maintaining the same range for the parameter  $b$ . In this case, it is observed that at all points of the

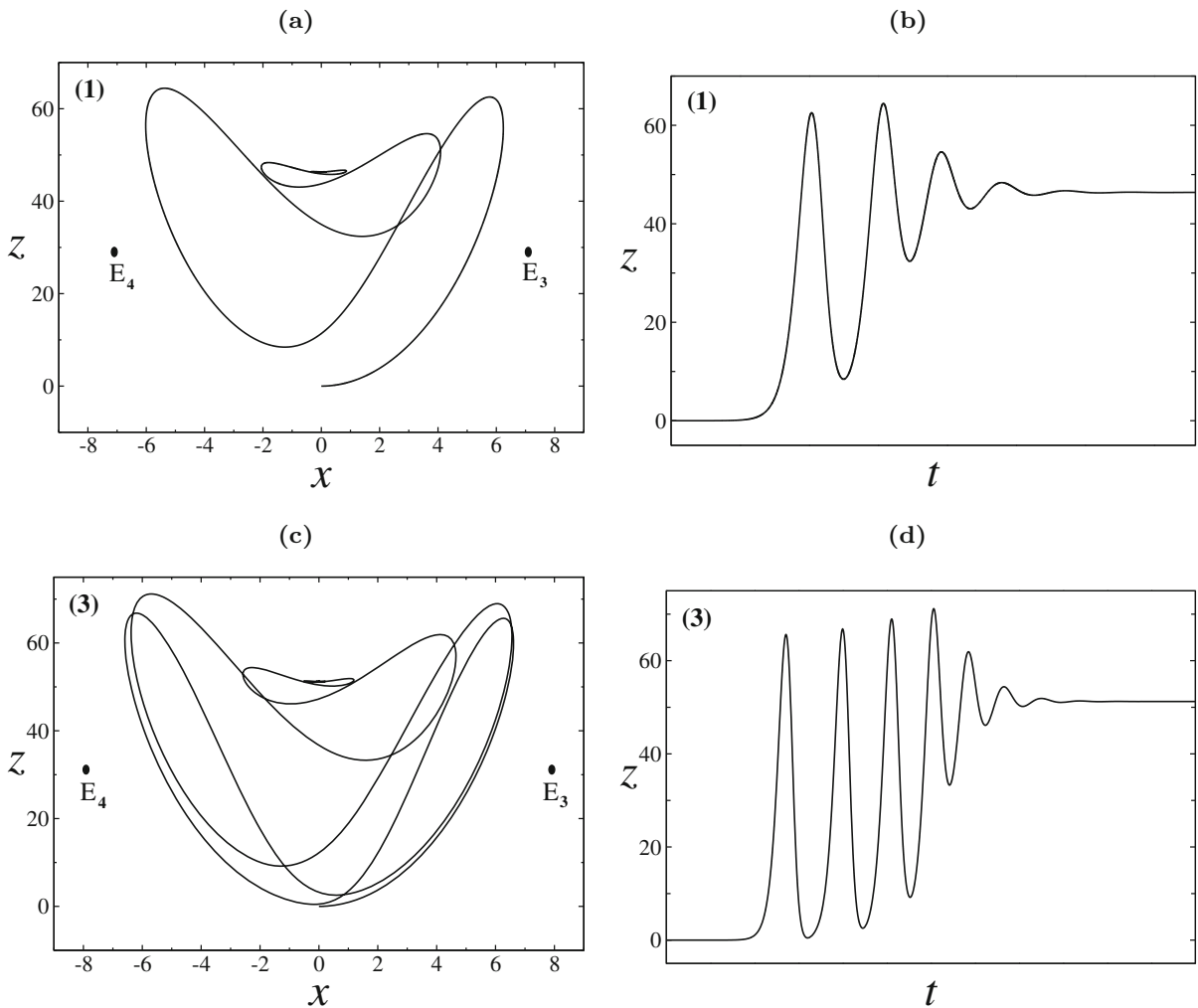


**Fig. 4** For  $\sigma = 0.3$ ,  $D = 0.1$ : **a** Projection on the  $(x, z)$ -plane of the heteroclinic orbit labelled **(1)** in Fig. 3d. **(b)** Temporal profile  $z(t)$  of heteroclinic orbit **(1)**. **(c)** Projection on the  $(x, z)$ -plane of the heteroclinic orbit labelled **(3)**. **(d)** Temporal profile  $z(t)$

of heteroclinic orbit **(3)**. Note that, to simplify the drawings, we have not included the heteroclinic connection located on the  $z$ -axis which joins  $E_2$  and  $E_1$  (it is structurally stable). This does appear drawn in Fig. 3f

curve **He**, since it arises from the degeneracy **DZ**, it is true that  $\delta_{12} < 1$ . As before, this graph presents a local maximum where a degeneration of the same type occurs as in the previous case. At this point **DHe<sup>2</sup>**, for  $(\rho, b) \approx (6.643798, 0.7443798)$  from the curve **He**, it is verified that  $\lambda_1^* = \lambda_2^* = -0.6$  and from that point on the heteroclinic cycle the equilibrium  $E_2$  changes from real saddle to saddle-focus. As a consequence of the above, and due to the continuity of the function  $\delta_{12}$  with respect to the parameters, there must exist a value in the three-parameter space  $(\rho, b, \sigma)$  where a

codimension-three degeneracy occurs, since the degeneracies **DHe<sup>2</sup>** and  $\delta_{12} = 1$  coincide at this point. Indeed, as can be seen in Fig. 5c at the point **DDHe<sup>2</sup>**, for  $(\rho, b, \sigma) \approx (6.1866153, 0.6915487, 0.2126370)$ , when  $D = 0.1$ , the heteroclinic cycle **He** undergoes a double degeneracy since the equilibrium  $E_2$  changes from real saddle to saddle-focus and also the product  $\delta_{12} = 1$ .

Now we fix  $\sigma = 0.4$ , that is, we move to the other side of the critical value  $\sigma = 1/3$ , where the degeneracy **DDZ** of the double-zero bifurcation of the origin

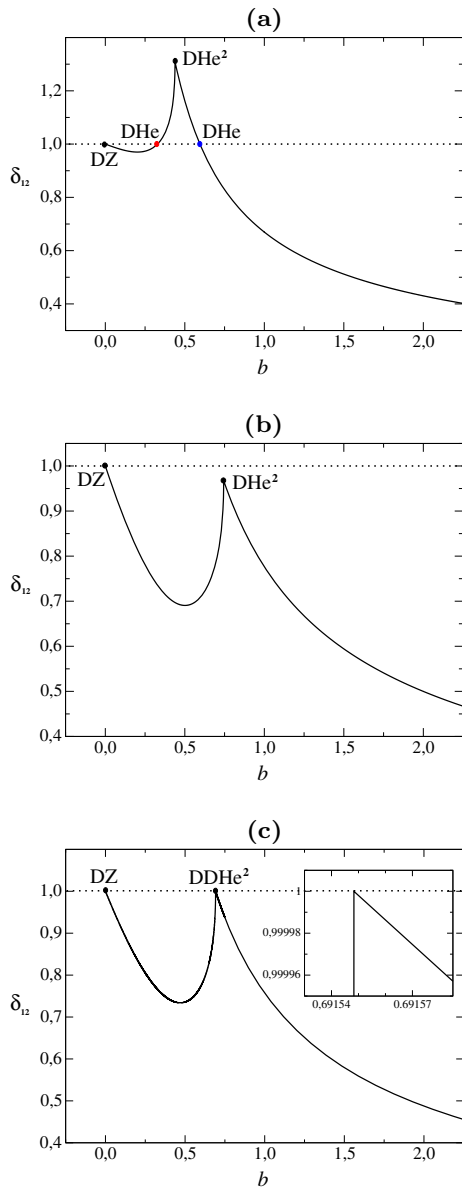


**Fig. 5** For  $D = 0.1$ , product of saddle quantities  $\delta_{12}$  versus parameter  $b$  on the points of the curve  $\mathbf{He}$  when: **a**  $\sigma = 0.3$ . **b**  $\sigma = 0.2$ . **c**  $\sigma \approx 0.212637$ . (Color figure online)

occurs. In Fig. 6a, we have represented the curves of Hopf bifurcation  $\mathbf{h}$  and of heteroclinic connections  $\mathbf{He}$ . Note that in the range shown in this figure these curves do not intersect and, in a neighborhood of the point  $\mathbf{DZ}$ , they have their positions exchanged with respect to those in Fig. 3a (since now the curve  $\mathbf{h}$  arises from  $\mathbf{DZ}$  to the left of the curve  $\mathbf{He}$ , as can be seen in Fig. 1 when  $\sigma > 1/3$ ). In addition, the Hopf bifurcation  $\mathbf{h}$

now appears supercritical, and at the point  $\mathbf{Dh}$ , for  $(\rho, b) \approx (4.4526922, 0.5295297)$ , it changes its character because another degeneracy  $a_1 = 0$  occurs. We note that this degeneracy is also present for  $\sigma = 0.3$  (it corresponds to the second point  $\mathbf{Dh}$  marked in Fig. 3a), but it is not related to the degenerate double-zero bifurcation  $\mathbf{DDZ}$  (the degeneracy  $\mathbf{Dh}$  appears due to the minimum of the curve  $\mathbf{Dh}$  with respect to  $\sigma$ , see Fig. 7). Indeed, when  $\sigma \approx 1/3$  this second degeneracy  $a_1 = 0$  is experienced at the point  $\mathbf{Dh}$  which occurs at  $(\rho, b) \approx (4.4094488, 0.5046604)$ .

As we can see in Fig. 6b, in a neighborhood of  $\mathbf{DZ}$ ,  $\delta_{12} > 1$  for this heteroclinic cycle. In this situation, the periodic orbit arising from the curve  $\mathbf{He}$  is attractive and, as expected, there is no longer a point on that curve where  $\delta_{12} = 1$  when both equilibria are real saddle. As in the previous case, in the region where  $\delta_{12} > 1$ , there is a point  $\mathbf{DHe}^2$ , which occurs at  $(\rho, b) \approx (3.0167880, 0.3241788)$ , where a maximum exists. At this point a double eigenvalue occurs,  $\lambda_1^* = \lambda_2^* = -0.7$ , and by increasing the value of  $b$ , the equilibrium  $E_2$  changes from real saddle to saddle-focus. In this zone we see that for  $\sigma = 0.4$  there is still a point  $\mathbf{DHe}$ , when  $(\rho, b) \approx (4.675, 0.5451430)$ , where  $\delta_{12} = 1$ . This fact confirms that this degeneracy is not related to  $\mathbf{DDZ}$ , as can be seen in Fig. 7. In fact, when  $\sigma \approx 1/3$  the degeneracy  $\delta_{12} = 1$ , being  $E_2$  a saddle-focus equilibrium, is experienced at  $(\rho, b) \approx (5, 0.5740328)$ .

In Fig. 6a, we have marked the degeneracy  $\mathbf{DHe}^2$  (as we said before, we conjecture that an infinite sequence of curves of homoclinic connections arises from it). We have also drawn the first curve of homoclinic connections of the origin  $\mathbf{Ho}$  (blue color) that emerges from  $\mathbf{DHe}^2$  (see the inset of Fig. 6a) and we have detected a degenerate point  $\mathbf{DHo}$ , which occurs at  $(\rho, b) \approx (9.1386649, 1.2353206)$ , where  $\lambda_3 = -\lambda_1 = -b$ , and consequently  $\delta_1 = 1$ . Although we have preferred not to draw it so as not to overcomplicate Fig. 6a, we remark that a second homoclinic connection to the origin arising from  $\mathbf{DHe}^2$  ends spiraling in a T-point  $\mathbf{TP}$ , which occurs at  $(\rho, b) \approx (15.3331808, 2.0863007)$ . As we are going to see in Sect. 4.2, the interaction between the curves emerged from the degenerate points  $\mathbf{DHe}^2$ ,  $\mathbf{DHo}$  and  $\mathbf{TP}$  is crucial to explain the disposition in the Lorenz system of the family of infinitely many homoclinic orbits previously found in the literature [51, Fig. 6], [52, Fig. 8B], [17, Fig. 3].

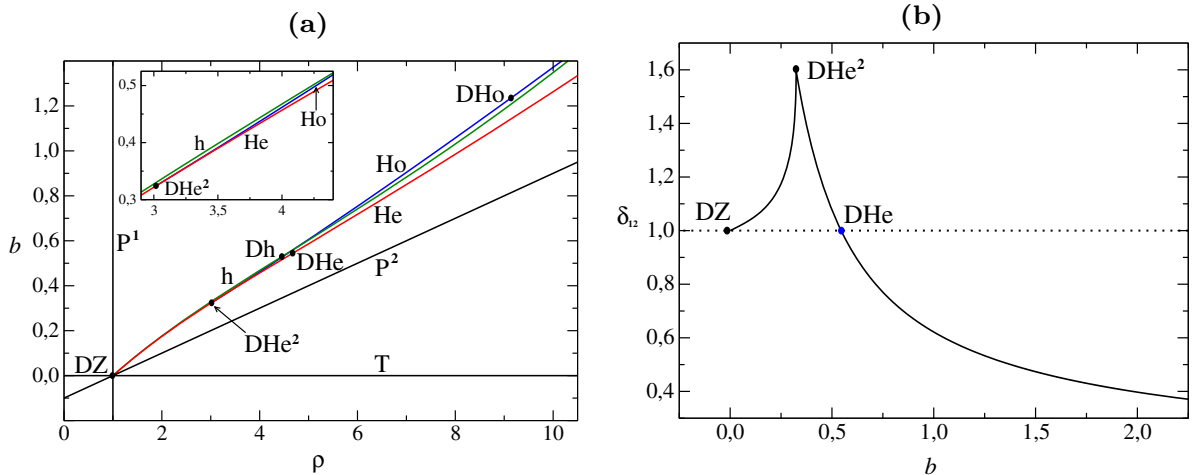


**Fig. 6** For  $\sigma = 0.4$ ,  $D = 0.1$ : **a** Partial bifurcation set in a neighborhood of the point **DZ**. Other four codimension-two bifurcations are also present: **Dh**, **DHe**, **DHe<sup>2</sup>** and **DHo**. **b** Product of

saddle quantities  $\delta_{12}$  versus parameter  $b$  on the points of the curve **He**. (Color figure online)

That is why, in the second part of this numerical study, we analyze the existence of the degeneracy **DHe<sup>2</sup>** when  $D = 0$  (Lorenz system). This will allow us to find its relationship with the sequence of homoclinic connections of the origin present in [17, Figs. 3–4], including the homoclinic connection that ends at the T-point heteroclinic loop **TP**.

Now we are going to determine in the  $(\rho, b, \sigma)$ -space, when  $D = 0.1$ , the loci where the degenerate bifurcations that we have found occur. We represent in Fig. 7 the projections onto the  $(\rho, \sigma)$ - and the  $(b, \sigma)$ -planes of the bifurcation curves corresponding to the four codimension-two degeneracies that exist in the first quadrant of Fig. 3a, namely **Dh** (degenerate Hopf bifurcation of the equilibria  $E_{3,4}$ ; green color), **DHe** (degeneracy condition  $\delta_{12} = 1$  on the curve of heteroclinic connections **He** between  $E_1$  and  $E_2$  when the equilibrium  $E_2$  is a real saddle (red color) and when it is a saddle-focus (orange color)), **DHe<sup>2</sup>** (degeneracy on the curve **He** when  $E_2$  changes from real saddle to saddle-focus; black color) and **DZ** (double-zero bifurcation of the equilibrium  $E_1$ ; blue color). We have also drawn the degeneracy **DHo** (degeneracy condition  $\delta_1 = 1$  on the curve of homoclinic connections of the origin **Ho**; magenta color) which we can see in Fig. 6a.

In Fig. 7, we observe that the curves **Dh** and **DHe** emerge from the point **DDZ** which occurs at  $(\rho, b, \sigma) = (1, 0, 1/3)$ . Remark that both curves are

tangent at **DDZ** and the equilibria  $E_1$  and  $E_2$  are real saddle.

The red curve **DHe** ends at the point **DDHe<sup>2</sup>**, which is located on the curve **DHe<sup>2</sup>**, being tangent to it. Let us remember that at **DDHe<sup>2</sup>** a double degeneracy occurs on the heteroclinic cycle **He** ( $\delta_{12} = 1$  and the equilibrium  $E_2$  changes from real saddle to saddle-focus). From that point, the other curve **DHe** (of equation (16) in the case of Fig. 7a, where  $\delta_{12} = 1$ ) also emerges. This curve is located to the right of the curve **DHe<sup>2</sup>**, in the area where the equilibrium  $E_2$  is saddle-focus, although in this case it is not tangent to the curve **DHe<sup>2</sup>** at **DDHe<sup>2</sup>**. Now we see that the two degenerate points **Dh**, that exist on the curve **h** in the range of Fig. 3a for  $\sigma = 0.3$ , belong to the same branch of the curve **Dh** and, due to a lack of transversality with respect to the parameter  $\sigma$ , these two degeneracies disappear when the value of  $\sigma$  decreases.

Finally, we note that on the curve **DHe<sup>2</sup>** there are other codimension-three degeneracies of the heteroclinic cycle **He**. Specifically, in Fig. 7 we have marked the point **DDHe<sup>12</sup>**, located at  $(\rho, b, \sigma) \approx (4.9938042, 0.5552146, 0.2511140)$ , where  $\delta_1 = 1$  (since  $\lambda_1 = -\lambda_3 = 1$ ). As can be seen, from **DDHe<sup>12</sup>** the curve **DHo** of degenerate homoclinic connections **Ho** emerges. We remark that  $\delta_1 < 1$  at the points of the curve **DHe<sup>2</sup>** above **DDHe<sup>12</sup>** while  $\delta_1 > 1$  for those below **DDHe<sup>12</sup>**. Thus,  $\delta_1 < 1$  at the points **DHe<sup>2</sup>** shown

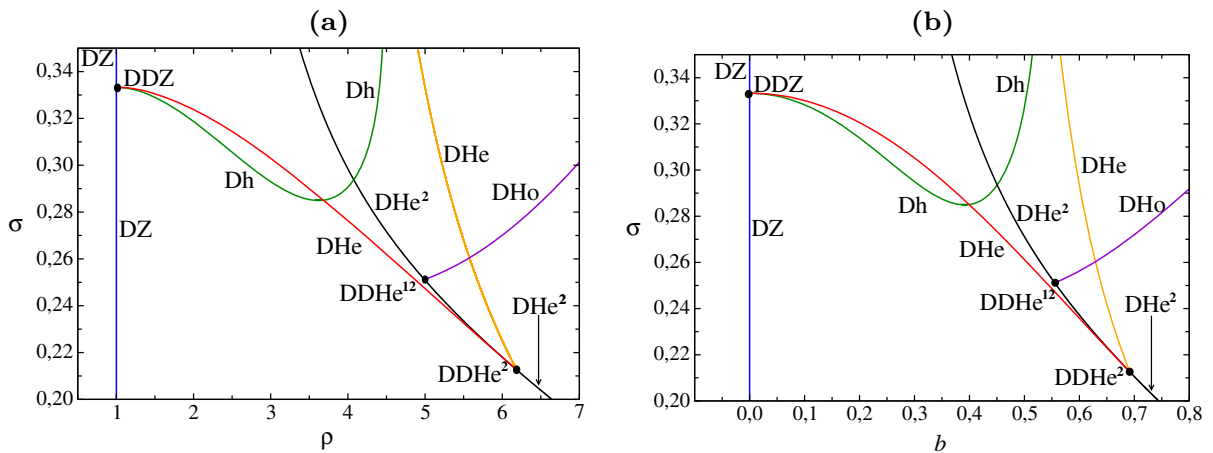


**Fig. 7** For  $D = 0.1$ , projection in the vicinity of the degenerate bifurcation point **DDZ** of the curves (**Dh** (degenerate Hopf bifurcation of the equilibria  $E_{3,4}$ ; green color), **DHe** (degeneracy condition  $\delta_{12} = 1$  on the curve of heteroclinic connections **He** when the equilibrium  $E_2$  is real saddle (red color), and when it is saddle-focus (orange color)), **DHe<sup>2</sup>** (degeneracy on the curve

**He** when  $E_2$  changes from real saddle to saddle-focus; black color), **DZ** (double-zero bifurcation of the equilibrium  $E_1$ ; blue color) and **DHo** (degeneracy  $\delta_1 = 1$  on the homoclinic connection to the origin; magenta color) onto: **a** the  $(\rho, \sigma)$ -plane. **b** the  $(b, \sigma)$ -plane. The codimension-three degeneracies **DDHe<sup>2</sup>** and **DDHe<sup>12</sup>** are also marked. (Color figure online)

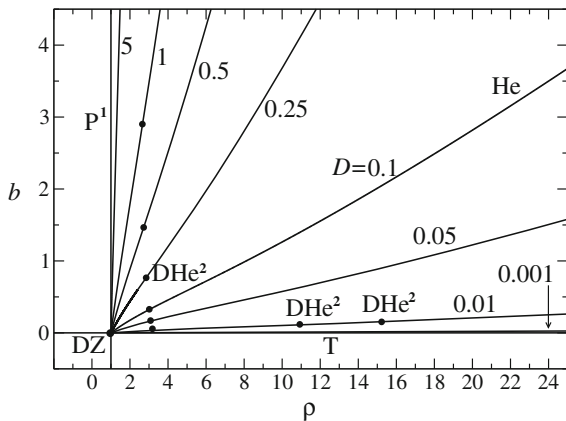


**Fig. 8** For  $\sigma = 0.4$ , curves of nondegenerate heteroclinic cycles **He**, related to **DZ**, for  $D = 0.001, 0.01, 0.05, 0.1, 0.25, 0.5, 1, 5$ , in the first quadrant of the  $(\rho, b)$ -plane. (Color figure online)

in Figs. 3a and 6a. As we are going to see in Sect. 4.2, the type of global bifurcations that emerge from **DHe<sup>2</sup>** will depend on the value of  $\delta_1$ .

Until now we have done our numerical study by setting  $D = 0.1$ . We are going to end this subsection by looking at how the curve **He** evolves when  $D$  varies. In Fig. 8, for  $\sigma = 0.4$ , we have represented in the  $(\rho, b)$ -plane the curves where the global connections **He** occur for the values  $D =$

0.001, 0.01, 0.05, 0.1, 0.25, 0.5, 1, 5. We recall that **DHe<sup>2</sup>** (marked with black bullets in this figure) corresponds to a degeneracy on the curve **He** because the equilibrium  $E_2$  changes from real saddle to saddle-focus.

As shown in Fig. 8, in the  $(\rho, b)$ -plane all the curves **He** arise from the double-zero degeneracy **DZ**. It is true that, setting a value of  $b$ , as the value of the  $D$  increases, the component  $z = \frac{b}{D} > 0$  of  $E_2$  decreases. Thus, this equilibrium approaches  $E_1$  and, as a consequence, the value of  $\rho$  in the points of the curves **He** corresponding to these heteroclinic cycles approaches the value  $\rho = 1$  where these cycles disappear. On the other hand, when  $D \rightarrow 0^+$ , the curves **He** are approaching the  $\rho$ -axis. This fact leads us to conjecture that the heteroclinic cycles corresponding to the value  $D = 0$  (Lorenz system) are located on the axis  $b = 0$  being therefore degenerate.

#### 4.2 Approaching the Lorenz system ( $D = 0$ )

The main objective of this subsection is to see how the global connections related to the double-zero bifurcation of system (2) allow to explain the origin of the global connection curves present in the partial bifurcation set found in the Lorenz system for  $\rho = 50$  (see

[17, Figs. 1 and 3]). We note that this complex distribution of the homoclinic connections in the Lorenz system has been previously found in the literature [51, 52], although the reason for this complicated behavior was unknown. Specifically, we want to analyze the evolution of these global connection curves when  $D \neq 0$  (keeping  $\rho = 50$ , we will start with  $D = 0.5$  and we will decrease the value of  $D$  until we reach  $D = 0$ ) and then to determine if some of the curves in the Lorenz system are related to the degeneracies found here on the curve **He**. In what follows, we will see that the degeneracies **DHe<sup>2</sup>**, **DHo** and **TP** play a key role in justifying the presence of the curves drawn in [17, Figs. 1 and 3] for the Lorenz system.

In Fig. 9a, we have represented a partial bifurcation set in the  $(b, \sigma)$ -parameter plane, for  $\rho = 50$ ,  $D = 0.5$  (three zooms of this bifurcation set appear in Fig. 9b–d). The curve **h** of supercritical Hopf bifurcation of  $E_{3,4}$ , given by (13), has a vertical asymptote when  $b = 2D(\rho - 1) = 49$  and ends at the point  $(b, \sigma) = (48, 0)$  (outside the range of the figure), since now the condition  $2D(\rho - 1) - b - \sigma - 1 \neq 0$  of (13) is not fulfilled. A degenerate point **DHe<sup>2</sup>**, which it placed at  $(b, \sigma) \approx (50.34911853, 204.78806517)$ , appears on the heteroclinic curve **He**. At this point the equilibrium  $E_2$  changes from real saddle to saddle-focus, whereas  $E_1$  is real saddle with  $\delta_1 > 1$ . From **DHe<sup>2</sup>**, as we said above, we conjecture that an infinite sequence of curves of homoclinic connections to the origin emerges, in addition to other bifurcation curves. We have only represented the first three curves of this infinite sequence, namely **Ho**, **Ho<sup>0</sup><sub>TP</sub>** and **Ho<sup>0</sup><sub>TPS</sub>**. The periodic orbits that arise from any of these homoclinic connections are attractive since  $\delta_1 > 1$  holds for all their points.

The notation we will employ from now on for the curves of homoclinic connections to the origin is similar to that used in [17]. On the one hand, we use a superscript to give information about the shape of the homoclinic orbit in the upper zone of the range of existence of the homoclinic curve (when it emerges from **DHe<sup>2</sup>**). On the other hand, the subscript informs about the shape of the homoclinic connection in the lower part of the region shown in the parameter plane (sometimes the curve ends in a codimension-two point and, in other cases, it leaves the region drawn in the figure). Specifically, in **Ho<sup>i</sup><sub>j</sub>**, the superscript  $i$  (the same explanation is valid for the subscript  $j$ ) indicates the number of turns around one of the non-trivial equilibria  $E_{3,4}$ , in our

case  $E_4$ , given by the projection in the  $(x, z)$ -plane of the homoclinic orbit whose leading unstable manifold arises towards the positive semi-axis  $x > 0$  (note that because of the symmetry a pair of the corresponding orbits exists).

The difference between the homoclinic connections corresponding to these three curves, **Ho**, **Ho<sup>0</sup><sub>TP</sub>** and **Ho<sup>0</sup><sub>TPS</sub>**, can be seen in Fig. 9e where we have drawn their projection on the  $(x, z)$ -plane for  $\sigma = 100$ . As can be observed, the homoclinic orbit corresponding to the curve **Ho** (green) whose leading unstable manifold arises towards the positive semi-axis  $x > 0$  does not cross the  $z$ -axis and reaches equilibrium  $E_1$  on its right hand side. On the contrary, the homoclinic orbit corresponding to the curve **Ho<sup>0</sup><sub>TP</sub>** (black) crosses the  $z$ -axis once (red line in the inset of Fig. 9e), close to  $E_2$  (black bullet), and enters  $E_1$  from its left side. For its part, the homoclinic orbit corresponding to the curve **Ho<sup>0</sup><sub>TPS</sub>** (blue) crosses the  $z$  axis twice before entering  $E_1$  on its right side. According to their shape, the corresponding superscript is “0” in the three cases (to simplify the notation of the principal homoclinic orbit to the origin we use **Ho** instead of **Ho<sup>0</sup><sub>0</sub>**). The curves **Ho<sup>0</sup><sub>TP</sub>** and **Ho<sup>0</sup><sub>TPS</sub>** end, respectively, at the principal T-point **TP**, which occurs at  $(b, \sigma) \approx (51.8873485, 14.3396057)$  (bullet orange), and at the secondary T-point **TPS**, situated at  $(b, \sigma) \approx (52.2305506, 6.8452189)$ . The projection onto the  $(x, z)$ -plane of these two heteroclinic cycles can be seen in Fig. 9f–g. Although in these two cases the subscript should be “ $\infty$ ” (because the homoclinic curves end spiraling at the T-points), we prefer to use “TP” and “TPS” to distinguish both curves.

As was the case with the heteroclinic connection curve in Fig. 3c, d, the curve **He** accumulates on a line segment on a saddle-node bifurcation curve of symmetric periodic orbits **SN<sub>1</sub>** (see Fig. 9b). This saddle-node curve arises from the cusp bifurcation point **CU**, which occurs at  $(b, \sigma) \approx (55.0074131, 11.8687941)$ . To the right of **CU** there is another bifurcation curve **SN<sub>2</sub>** of the same type.

In what follows, we are going to focus on seeing the evolution of the curves **Ho** and **Ho<sup>0</sup><sub>TP</sub>** as well as of other new homoclinic curves which, as we will see, emerge from **DHe<sup>2</sup>** (we will no longer show the curve **Ho<sup>0</sup><sub>TPS</sub>** because it is not relevant to the results we present). Thus, keeping  $\rho = 50$ , we decrease the value of the parameter to  $D = 0.21$  and draw the partial bifurcation set of Fig. 10a. As in Fig. 9a, the bifurcation curves **h**, **He**, **Ho** and **Ho<sup>0</sup><sub>TP</sub>** are also present. The Hopf

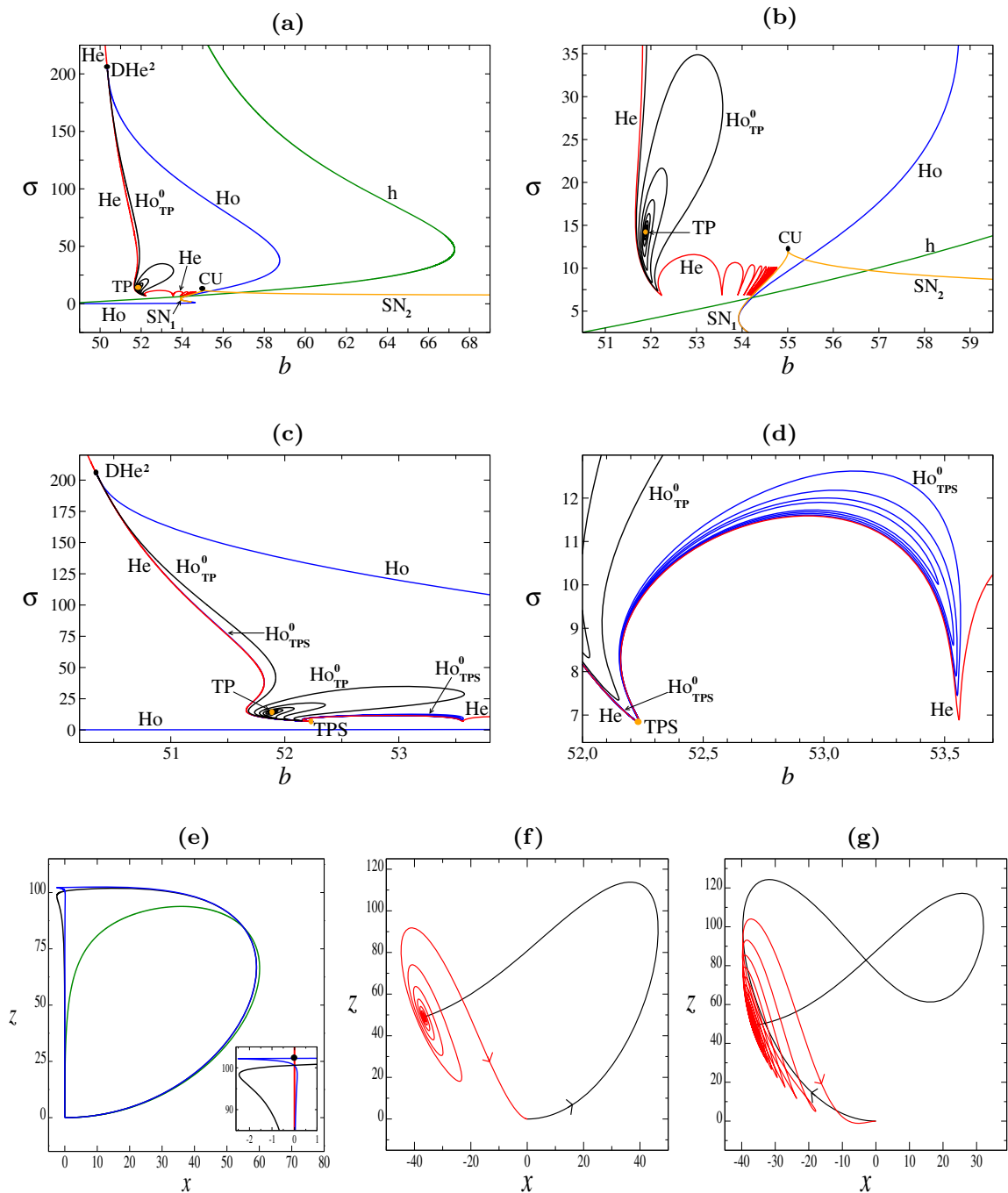


**Fig. 9** For  $\rho = 50, D = 0.5$ : **a** Partial bifurcation set in the  $(b, \sigma)$ -plane with the curves **h** (supercritical Hopf bifurcation of the nontrivial equilibria  $E_{3,4}$ ; green), **Ho**, **Ho<sub>TP</sub><sup>0</sup>** (homoclinic connections to the origin; blue and black, respectively), **He** (heteroclinic connections between  $E_1$  and  $E_2$ ; red) **SN<sub>1</sub>** and **SN<sub>2</sub>** (saddle-node bifurcations of symmetric periodic orbits; orange). **b–d** Zooms of panel (a) including the curve **Ho<sub>TPS</sub><sup>0</sup>** (blue) of homoclinic connections to the origin. Projection onto the  $(x, z)$ -

plane of the: **e** homoclinic connections to the origin **Ho** (green), **Ho<sub>TP</sub><sup>0</sup>** (black) and **Ho<sub>TPS</sub><sup>0</sup>** (blue), for  $\sigma = 100$ ; **f** principal T-point **TP** between  $E_1$  and  $E_4$  (note that because of the symmetry a pair of the corresponding orbits exists); **g** secondary T-point **TPS** between  $E_1$  and  $E_4$ . The black line corresponds to the intersection between the one-dimensional manifolds of the equilibria  $E_1$  and  $E_4$  and the red one to the intersection between the two-dimensional manifolds. (Color figure online)

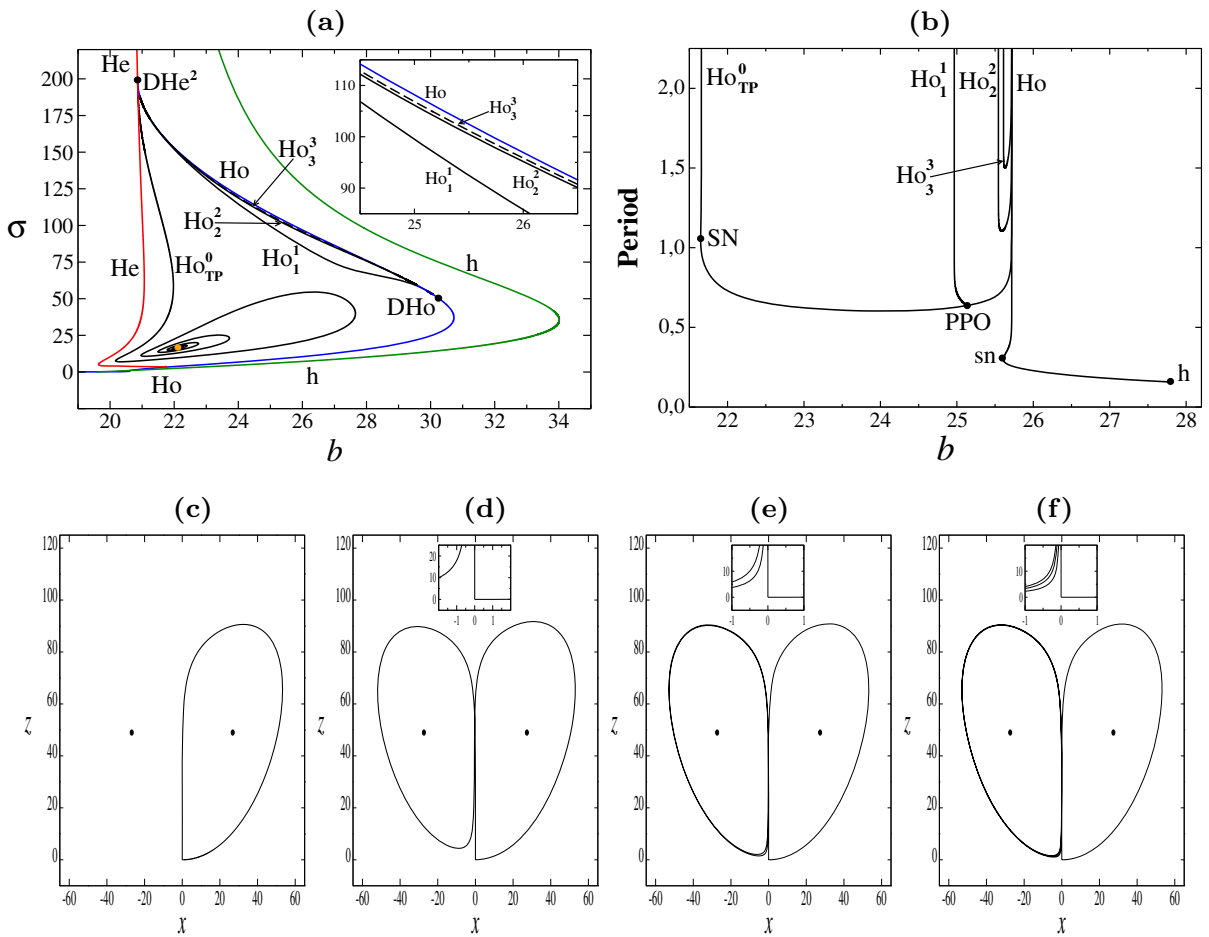


**Fig. 10** For  $\rho = 50$ ,  $D = 0.21$ : **a** Partial bifurcation set in the  $(b, \sigma)$ -plane with the curves **h** (Hopf bifurcation of the non-trivial equilibria  $E_{3,4}$ ), **Ho**, **Ho<sub>1</sub><sup>1</sup>**, **Ho<sub>2</sub><sup>2</sup>**, **Ho<sub>3</sub><sup>3</sup>**, **Ho<sub>TP</sub><sup>0</sup>** (curves of homoclinic orbits to the origin) and **He** (heteroclinic connection between  $E_1$  and  $E_2$ ). The principal T-point is marked with an orange bullet. **b** For  $\sigma = 100$ , bifurcation diagram of the sym-

metric and asymmetric periodic orbits that end at **Ho** and of the asymmetric periodic orbits emerged from **h**, **Ho<sub>1</sub><sup>1</sup>**, **Ho<sub>2</sub><sup>2</sup>** and **Ho<sub>3</sub><sup>3</sup>**. For  $\sigma = 100$ , projection onto the  $(x, z)$ -plane of the homoclinic orbit corresponding to the curve: **c Ho** for  $b \approx 25.7178751$ ; **d Ho<sub>1</sub><sup>1</sup>** for  $b \approx 24.965864$ ; **e Ho<sub>2</sub><sup>2</sup>** for  $b \approx 25.543696$ ; **f Ho<sub>3</sub><sup>3</sup>** for  $b \approx 25.610137$ . (Color figure online)

bifurcation curve **h** now ends, for the same reason as before, at the point  $(b, \sigma) = (19.58, 0)$ , and the point of codimension two **DHe<sup>2</sup>** continues to exist on the curve **He**, for  $(b, \sigma) \approx (20.8579428, 199.2891303)$ . However, while  $E_1$  is still a real saddle, now  $\delta_1 < 1$  (which implies an important change as we will discuss below). From point **DHe<sup>2</sup>** the homoclinic connections to the origin **Ho<sub>TP</sub><sup>0</sup>** and **Ho** continue to emerge but, as can be seen in the figure, a new degeneration **DHo** appears on the curve **Ho**, when  $(b, \sigma) \approx (30.2447608, 50.3854047)$ . At this point,  $\delta_1 = 1$  (since  $\lambda_2 < \lambda_3 = -\lambda_1 = -b$ ). So, from **Ho**, a non-stable

periodic orbit arises between the points **DHe<sup>2</sup>** and **DHo** (since  $\delta_1 < 1$ ) whereas this periodic orbit is stable below the point **DHo** ( $\delta_1 > 1$ ). As a consequence of this, for this value of  $D$  there is a new infinite sequence  $\{\mathbf{Ho}_i^i\}$  of homoclinic connections to the origin (apart from other bifurcation curves such as saddle-node of periodic orbits, symmetry-breaking of symmetric periodic orbits, etc.) that join **DHe<sup>2</sup>** and **DHo**. In Fig. 10a we have represented the first three curves of the sequence, namely **Ho<sub>1</sub><sup>1</sup>**, **Ho<sub>2</sub><sup>2</sup>** and **Ho<sub>3</sub><sup>3</sup>** (dashed line).

As seen in Fig. 10d–f, for  $\sigma = 100$ , these homoclinic connections are different from those that exist

in the **Ho** (see Fig. 10c) and **Ho<sub>TP</sub>** curves (see Fig. 9e) in the sense that their projection onto the  $(x, z)$ -plane surrounds both non-trivial equilibria  $E_{3,4}$  (black bullets). Note that, although we have not represented them in Fig. 10a, on the curve **Ho<sub>TP</sub>** there are several points **DHo** (the intersection points of this curve with the curve  $\delta_1 = 1$ ), where the same degeneracy present on curve **Ho** is experienced.

To see the relationship that exists between the periodic orbits that arise from these homoclinic connections, and justify the previously mentioned difference, we draw in Fig. 10b the bifurcation diagram for  $\sigma = 100$ . An asymmetric non-stable periodic orbit arises from **Ho**, which after undergoing a saddle-node bifurcation of periodic orbits **sn** (for  $b \approx 25.6078095$ ) disappears as a stable periodic orbit at the supercritical Hopf bifurcation **h**. Due to the symmetry, a non-stable symmetric periodic orbit also arises from **Ho** [67], which undergoes a symmetry-breaking bifurcation **PPO**, for  $b \approx 25.1363078$ . The attractive periodic orbit arising from **PPO** undergoes a saddle-node bifurcation **SN** in which it becomes a saddle. Finally, it ends in the homoclinic connection **Ho<sub>TP</sub>**.

The saddle asymmetric periodic orbit that emerges from the bifurcation **PPO** is the one that ends in the homoclinic connection **Ho<sub>1</sub>** and, as it arises from the symmetry breaking of a symmetric periodic orbit whose projection on the  $(x, z)$ -plane surrounds both non-trivial equilibria  $E_{3,4}$ , the projection of this homoclinic connection also does. Finally, the saddle asymmetric periodic orbits arising from **Ho<sub>2</sub>** and **Ho<sub>3</sub>** also end, without undergoing any bifurcation, on the homoclinic connection **Ho**. Consequently, this is an example of a system in which infinitely many periodic orbits bifurcate from a homoclinic connection to a real saddle ( $\delta < 1$ ) and its theoretical analysis has not yet been carried out. Note that this is not surprising since an infinite number of saddle periodic orbits is born right after the homoclinic-butterfly bifurcation (a pair of homoclinic orbits to the origin) with a saddle equilibrium with  $\delta < 1$  [68,69].

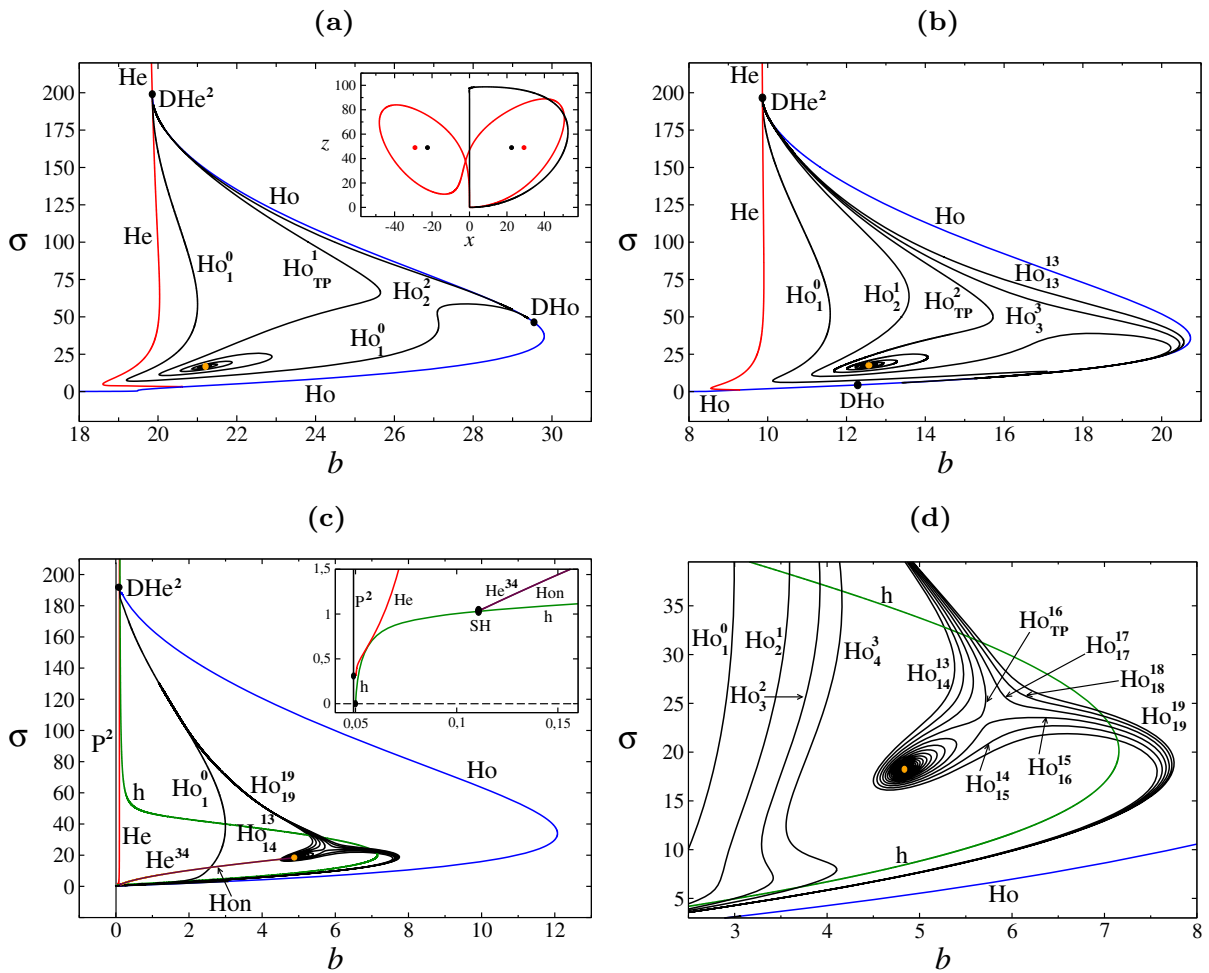
The three-parameter continuation of **DHo** allows to detect that, for  $\rho = 50$ , there is a codimension-three degeneracy on the curve **He** when  $(b, \sigma, D) \approx (40.6626754, 203.1965805, 0.4054090)$ . At this point, **He** exhibits a double degeneracy since  $\delta_1 = 1$  for  $E_1$  and, simultaneously,  $E_2$  changes from real saddle to saddle-focus. We called **DDHe<sup>12</sup>** to this codimension-three degeneracy when we found it for  $D = 0.1$  (see

Fig. 7) which, as far as we know, has not been studied in the literature either. We note that the points where the equilibrium  $E_1$  fulfills that  $\delta_1 = 1$  do not depend on the value of the parameter  $D$ .

As a consequence, when  $D < D_c \approx 0.4054090$ , the point **DHo** appears on the curve **Ho** in the  $(b, \sigma)$ -plane. This implies that, in this parameter plane, the bifurcations related to the degeneracy **DHe<sup>2</sup>** are different on each side of the value  $D_c$ . Specifically, new bifurcation curves emerge from **DHe<sup>2</sup>** when  $D < D_c$  (for example, those of the new sequence of homoclinic connections of the origin **Ho<sub>i</sub>**) since now  $\delta_1 < 1$  for the equilibrium  $E_1$ .

Next, to try to explain the origin of the curves that appear in [17, Figs. 1–4] for Lorenz system ( $D = 0$ ), we investigate in Fig. 11 how the bifurcation set evolves as  $D$  decreases.

When  $D = 0.2$ , we see in Fig. 11a how a contact has already been produced between the curves **Ho<sub>1</sub>** and **Ho<sub>TP</sub>** of Fig. 10a. This implies that although these curves of homoclinic connections continue to emerge from the point **DHe<sup>2</sup>**, placed at  $(b, \sigma) \approx (19.8533783, 199.0625408)$ , they have swapped the points of the parameter plane where they now end. Thus, **Ho<sub>1</sub>** ends in **DHo**, situated at  $(b, \sigma) \approx (29.5439568, 46.3809284)$  and **Ho<sub>TP</sub>** does it in **TP** (orange bullet), located at  $(b, \sigma) \approx (21.2063502, 16.809238)$ . We note that the contact between the curves **Ho<sub>TP</sub>** and **Ho<sub>1</sub>** occurs near the point **DHo**, in a zone where these homoclinic connections are orientable. The tangency takes place between **Ho<sub>1</sub>** and the outer loop of the spiral curve **Ho<sub>TP</sub>**, since, in this zone, the projection on the  $(x, z)$ -plane of the homoclinic orbit corresponding to these values gives a turn to each of the equilibria  $E_{3,4}$ . Let us remember that although initially, when it arises from **DHe<sup>2</sup>**, the projection of the homoclinic orbit corresponding to the curve **Ho<sub>TP</sub>** only surrounds one of the equilibria  $E_{3,4}$ , in our case  $E_3$  (see Fig. 9e), later the homoclinic orbit turns around the same equilibrium, in our case  $E_4$ , one more time (in the phase space) as the curve turns one more time (in the parameter plane) in its spiraling way towards the T-point. In the inset of Fig. 11a, to illustrate the evolution of the homoclinic orbits along the curve **Ho<sub>1</sub>**, we show the projection onto the  $(x, z)$ -plane of two of them. The first one (in black), for  $\sigma = 150, b \approx 20.0900594$ , is “close to” **DHe<sup>2</sup>** (its shape justifies the superscript “0”) whereas the second one (in red),  $\sigma = 50, b \approx 27.0985454$ , is “close to”



**Fig. 11** For  $\rho = 50$  partial bifurcation set in the  $(b, \sigma)$ -plane: **a** for  $D = 0.2$ ; **b** for  $D = 0.1$ ; **c** for  $D = 0.001$ . **d** Zoom of panel (c) in the vicinity of the T-point. (Color figure online)

**DHo** (its shape justifies the subscript “1”). Equilibria  $E_{3,4}$  are also marked in the corresponding colors.

In Fig. 11b we see how, by decreasing the value of the parameter to  $D = 0.1$ , the same contact process has been repeated between the curve  $\mathbf{Ho}_2^2$  (whose projection on the  $(x, z)$ -plane gives two turns to the equilibrium  $E_4$  according to Fig. 10e) and the outer loop of the spiral curve  $\mathbf{Ho}_{TP}^1$  of Fig. 11a, whose homoclinic orbits have a projection with the same number of turns to each of the equilibria  $E_{3,4}$ . As a consequence, there is a new curve of homoclinic connections  $\mathbf{Ho}_2^1$  that, like the curve  $\mathbf{Ho}_1^0$ , goes from the point  $\mathbf{DHe}^2$ , located at  $(b, \sigma) \approx (9.8657655, 196.6255324)$ , to the point  $\mathbf{DHo}$ , situated at  $(b, \sigma) \approx (12.2833185, 4.4438448)$ . We also draw in Fig. 11b the curves of homoclinic con-

nections  $\mathbf{Ho}_3^3$  and  $\mathbf{Ho}_{13}^{13}$  that are orientable at all points. Between these two curves are located the curves  $\mathbf{Ho}_i^i$  ( $i = 4, 5, \dots, 12$ ) which we have not drawn so as not to overload the figure excessively.

Since we want to keep decreasing  $D$  to get closer to  $D = 0$ , in Fig. 11c we have drawn a partial bifurcation set for  $D = 0.001$ . In this case we have included the curve  $\mathbf{P}^2$  where a pitchfork bifurcation of the equilibrium  $E_2$  takes place when  $b = D(\rho - 1) = 0.049$ . The Hopf bifurcation curve  $\mathbf{h}$  has a vertical asymptote at  $b = 2D(\rho - 1) = 0.098$  and ends by contacting the  $b$  axis at the point  $(b, \sigma) = (0.04998, 0)$ , since now the condition  $b(\rho + \sigma) - 2D(\rho - 1)\sigma + D(1 - \rho^2) > 0$  of (13) is not fulfilled (see the inset of Fig. 11c). In agreement with what was obtained in Fig. 8 the curve

of heteroclinic cycles **He** is close to the axis  $b = 0$ , presenting a vertical asymptote for  $b \approx 0.0979964$  very close to the asymptote of the curve **h**. In this case the degeneracy **DHe**<sup>2</sup> continues to exist and is placed at  $(b, \sigma) \approx (0.09796673, 193.8617781)$ . In the region between **Ho** and **Ho**<sup>0</sup> we have drawn (see Fig. 11c–d) the curves **Ho**<sub>14</sub><sup>13</sup>, **Ho**<sub>15</sub><sup>14</sup>, **Ho**<sub>16</sub><sup>15</sup>, **Ho**<sub>TP</sub><sup>16</sup>, **Ho**<sub>17</sub><sup>17</sup>, **Ho**<sub>18</sub><sup>18</sup> and **Ho**<sub>19</sub><sup>19</sup>, which all arise from the point **DHe**<sup>2</sup>.

As we can see, the curve **Ho**<sub>TP</sub><sup>16</sup>, whose orbit makes 16 turns around  $E_4$  when it arises from **DHe**<sup>2</sup>, is the one that now ends at the T-point **TP** (orange bullet), placed at  $(b, \sigma) \approx (4.837184, 18.241456)$ . As can be seen in the inset of Fig. 11c, the curves **Hon** (homoclinic connections to  $E_{3,4}$ ) and **He**<sup>34</sup> (heteroclinic connections between  $E_3$  and  $E_4$ ) arise from the point **TP**, with the shape predicted in [11]. As in the Lorenz system, these two curves are so close as to be almost indistinguishable. They end in Shil’nikov-Hopf degenerate points **SH** [17, 70] when they intersect the Hopf curve **h** at  $(b, \sigma) \approx (0.1103258, 1.0293202)$ . In the zoom of Fig. 11d we have also included the first four curves of homoclinic connection **Ho**<sub>1</sub><sup>0</sup>, **Ho**<sub>2</sub><sup>1</sup>, **Ho**<sub>3</sub><sup>2</sup> and **Ho**<sub>4</sub><sup>3</sup> (in order not to complicate this figure too much, we have not included the curves **Ho**<sub>5</sub><sup>4</sup>, **Ho**<sub>6</sub><sup>5</sup>, ..., **Ho**<sub>13</sub><sup>12</sup> which are placed consecutively between **Ho**<sub>4</sub><sup>3</sup> and **Ho**<sub>14</sub><sup>13</sup>).

In Fig. 12a we consider  $D = 0$  (Lorenz system). Now the Hopf curve **h** is bounded and exists between the points  $(b, \sigma) \approx (0, 1.089065)$  and  $(b, \sigma) \approx (0, 45.910935)$ , where the condition  $b(\rho + \sigma) > 0$  is not satisfied (see [48]). Furthermore, in this case we know that the curve of heteroclinic cycles **He** no longer exists in the  $(b, \sigma)$ -plane, although there are infinitely many heteroclinic orbits (placed outside the  $z$ -axis) joining points of the continuum of equilibria  $E_z = (0, 0, z)$ ,  $z \in \mathbb{R}$ , that exists on the  $z$ -axis when  $b = 0$  [59]. Thus, the three-parameter continuation in the  $(b, \sigma, D)$ -space of the point **DHe**<sup>2</sup> of the Fig. 11c for  $D = 0.001$  allows us to obtain the point **DHe**<sub>\*</sub><sup>2</sup>, placed at  $(b, \sigma_*, D) \approx (0, 193.8318321, 0)$ . For  $\rho = 50$ , as the value of  $\sigma$  reaches  $\sigma_*$ , the equilibrium point  $E_{z_*} \approx (0, 0, 97.9592478)$  has a double degeneracy since it has a nonzero double eigenvalue and a zero eigenvalue. Remember that when  $b = 0$  the eigenvalues of the equilibria  $E_z$  are [14]

$$\begin{aligned} \lambda_{1,2} &= \frac{-(1 + \sigma) \pm \sqrt{(1 + \sigma)^2 + 4\sigma(\rho - z - 1)}}{2}, \\ \lambda_3 &= 0. \end{aligned} \tag{17}$$

The heteroclinic orbit connecting the origin and the non-isolated equilibrium  $E_{z_*}$  is represented in Fig. 12b, labeled 2.

For  $\rho = 50$ ,  $\sigma = \sigma_*$ , there are still infinitely many heteroclinic orbits and, among all of them, the one that arises from the origin ends at  $E_{z_*}$ , which has a nonzero double eigenvalue  $\lambda_1 = \lambda_2 = \frac{-(1 + \sigma_*)}{2} \approx -97.4159$ ,  $\lambda_3 = 0$ . Likewise, the equilibrium  $E_{z_0}$ , where  $z_0 = \rho - 1 = 49$ , has a double-zero eigenvalue. The eigenvalues of the rest of the infinite equilibria satisfy  $\lambda_2 < \lambda_3 = 0 < \lambda_1$  (“zero-saddle”) for  $z < z_0$ ,  $\lambda_2 < \lambda_1 < \lambda_3 = 0$  (“zero-node”) when  $z_0 < z < z_*$  and  $\lambda_{1,2} = \alpha \pm i\beta$  ( $\alpha < 0$ ,  $\beta \neq 0$ ),  $\lambda_3 = 0$  (“zero-focus”) if  $z > z_*$ .

We note that the equilibrium  $E_{z_0}$  organizes the infinite heteroclinic orbits that join two points of the  $z$ -axis, in the sense that all these heteroclinic orbits arise from points  $E_z$  with  $z < z_0$  (“zero-saddle”) and end at points  $E_z$  with  $z > z_0$  (“zero-node” if  $z < z_*$  or “zero-focus” when  $z > z_*$ ). In Fig. 12b we have also drawn two representative heteroclinic orbits. One (label 1) starts at  $z = 20$  ( $0 < z$ ) and ends at a point with  $z_0 < z < z_*$  (this equilibrium is a “zero-node”) and the other (label 3) starts at  $z = -20$  ( $z < 0$ ) and ends at an equilibrium point with  $z_* < z$  (this is a “zero-focus” and consequently the heteroclinic orbit approaches this point in a spiral way, as can be noticed in the zoom).

The key fact is that, when we perturb the Lorenz system with  $D \neq 0$ , the only heteroclinic orbit that continues to exist is the one that joins the origin  $E_1$  with  $E_2$  (the only equilibria that exist on the  $z$ -axis). Note that when  $b = D = 0$ , the eigenvalues  $(\lambda_1, \lambda_2, \lambda_3)$  of the equilibrium points  $E_z$ , including that of  $E_{z_*}$ , are the same as the eigenvalues of  $E_2 = (0, 0, b/D)$  when  $b, D \neq 0$  (see (14)), if we take  $z = b/D$  in Eq. (17).

For other values of  $\sigma$  (when  $b = D = 0$ ), we have found numerical evidence that the heteroclinic connection leaving the origin ends in another equilibrium but which does not have a double eigenvalue. Also, a heteroclinic orbit still exists between two equilibria of the  $z$ -axis, where the upper equilibrium (with  $z > z_0$ ) has a double eigenvalue but the lower equilibrium (with  $z < z_0$ ) is not the origin.

The numerical continuation of the curves **Ho**<sub>i</sub><sup>j</sup> of Fig. 12c shows that all of them arise from the degeneracy **DHe**<sub>\*</sub><sup>2</sup>. Also, as can be seen in Fig. 12d, the curve **Ho**<sub>TP</sub><sup>17</sup> ends at the principal T-point, in agreement with the result obtained in [17, Figs. 3–4]. This indicates that there is a parameter value  $D \in (0, 0.001)$  where there

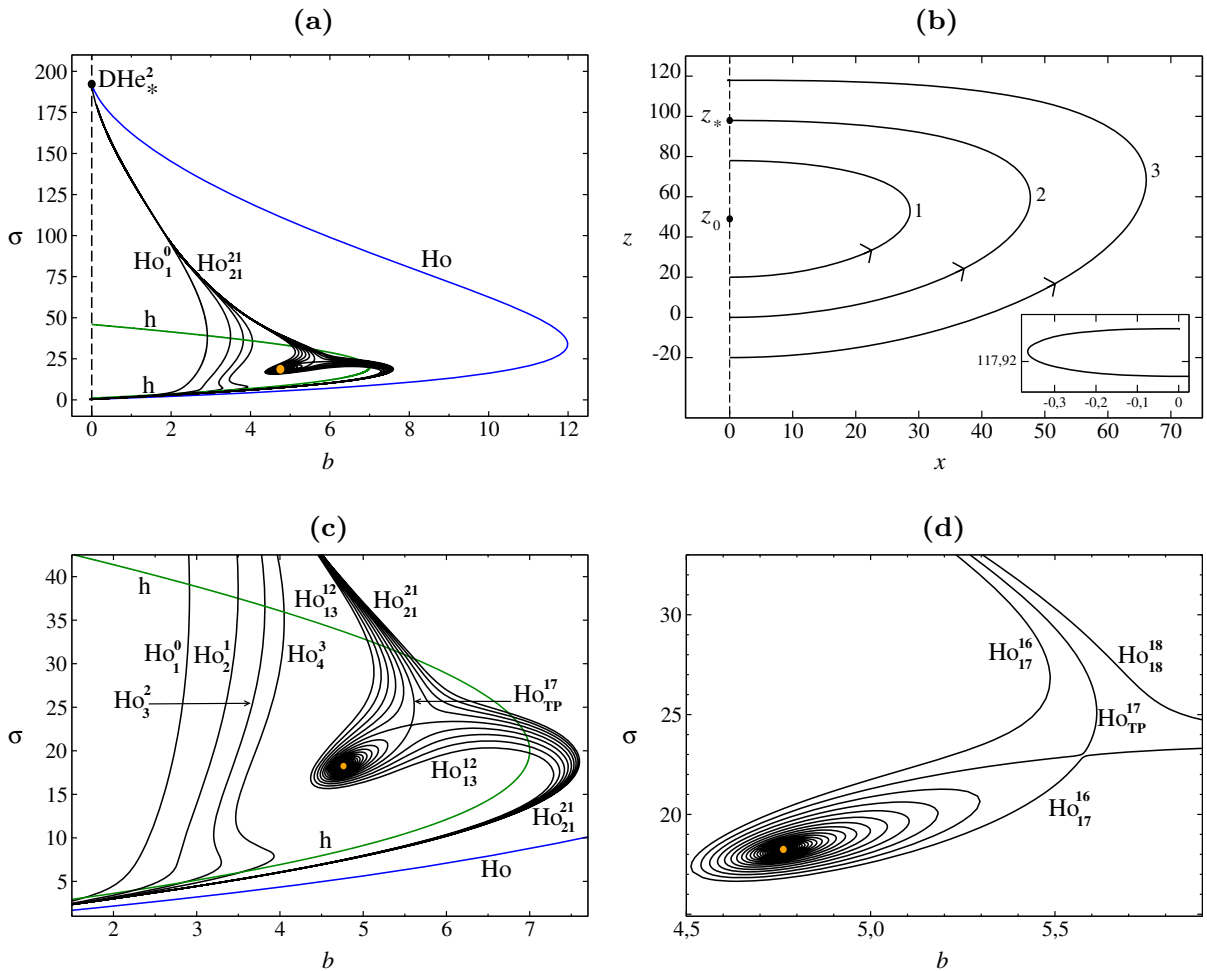


**Fig. 12** **a** For  $\rho = 50$ ,  $D = 0$ , partial bifurcation set in the  $(b, \sigma)$ -plane. **b** Projection on the  $(x, z)$ -plane of heteroclinic orbit (label 2) corresponding to point  $DHe_*^2$  in panel (a). The heteroclinic orbits that start at  $z = 20$  (label 1) and at  $z = -20$  (label

3) are also represented. One zoom of this last orbit in the vicinity of its endpoint (a “zero-focus”) is also drawn. **c** Zoom of panel (a) in the vicinity of the T-point (orange bullet). **d** Zoom of panel (c). (Color figure online)

has been a contact between the curves  $Ho_{TP}^{16}$  and  $Ho_{17}^{17}$  of Fig. 11d, giving rise to the new curves  $Ho_{17}^{16}$  and  $Ho_{TP}^{17}$  drawn in Fig. 12. Finally we note that the bifurcation set of Fig. 11c, d, for  $D = 0.001$ , is similar to that of [17, Fig. 4b], corresponding to  $\rho = 50.1$ . This tells us that, given  $\rho = 50$ , decreasing the value of the parameter  $D$  (transition from  $D = 0.001$  to  $D = 0$ ) in system (2) produces on the curves  $Ho_j^i$ , the same effect as that obtained when the value of  $\rho$  is decreased (transition from  $\rho = 50.1$  to  $\rho = 50$ ) in Lorenz system (1).

### 5 Conclusions

In this work, given the difficulties that appear to study the double-zero bifurcation in the Lorenz system (because it is exhibited by a non-isolated equilibrium), we propose the new system (2) which encompasses the Lorenz system. To do this we add the term  $Dz^2$  in the third equation and, since the continuum of equilibria disappears, it is already possible to study the double-zero bifurcation. Once we have shown that the double-zero degeneracy of the origin guarantees, in a certain region of the parameter space, the existence of heteroclinic cycles (see Theorem 1), we carry out a numerical

study to see how that heteroclinic connection evolves as it separates from the singularity.

At first, in Sect. 4.1, we have moved to either side of a degeneracy of the double-zero bifurcation which occurs when  $\sigma = 1/3$ . This has allowed us to find that the curve of heteroclinic connections accumulates on a line segment of the saddle-node curve  $\text{SN}_1$  (see Fig. 3d). As far as we know, this is the first example in which the accumulation process occurs in the region in which the periodic orbit involved in the saddle-node bifurcation does not exist. Thus, the heteroclinic cycle accumulates on a non-hyperbolic periodic orbit. In addition, we have found the following global bifurcations of codimension two (see Fig. 7):

- **DHe**, degenerate heteroclinic connection because  $\delta_{12} = 1$ , being  $E_2$  a real saddle equilibrium. This curve joins points **DDZ** and **DDHe<sup>2</sup>**. In the parameter plane, a curve of saddle-node bifurcations emanates from **DHe**. We note that from this point **DDHe<sup>2</sup>** arises another degeneracy **DHe**, degenerate heteroclinic connection because  $\delta_{12} = 1$ , being  $E_2$  a saddle-focus equilibrium.
- **DHe<sup>2</sup>**, degenerate heteroclinic connection because  $E_2$  changes from real saddle to saddle-focus (the double real eigenvalue is negative). As far as we know, this degeneracy has not been studied in the literature. From the numerical results we have found, we conjecture the existence of an infinite sequence of bifurcation curves of various types that emanate from this point: saddle-nodes of asymmetric and symmetric periodic orbits, period-doublings of the asymmetric periodic orbits, symmetry-breakings of the symmetric periodic orbits, homoclinic connections of the origin,... (recall that a similar scenario appears in a Belyakov bifurcation [71–74], exhibited by a homoclinic connection at an equilibrium point in  $\mathbb{R}^3$  where a pair of eigenvalues change from real to complex; it seems that the point **DHe<sup>2</sup>** is a “heteroclinic analogue” of the so-called Belyakov point). Remark that two degeneracies **DDHe<sup>2</sup>** and **DDHe<sup>12</sup>** appear on this curve. **DHe<sup>2</sup>** exhibits even greater bifurcation richness when  $\delta_1 < 1$ .
- **DHo**, degenerate homoclinic connection of the origin because  $\delta_1 = 1$ , being a real saddle. In the generic situation for a neutral resonant saddle (see [31, Sect. 2.2.1] and [32, Theorem 5.13]) there are two possibilities. If the homoclinic orbit is non-

twisted, an extra curve of saddle-node bifurcation of periodic orbit appears whereas if it is twisted, two curves originate at the critical point (which correspond to a double homoclinic orbit and to a period-doubling bifurcation). However, the bifurcation scenario we have found here is much more complicated (we conjecture that infinitely many curves appear, see Figs. 10a, 11b) and it deserves to be studied theoretically in the near future. It seems that the structurally stable heteroclinic connection along the  $z$ -axis between  $E_2$  and the origin affects the bifurcations involved at this singularity. Remark that the curve **DHo** emerges from the point **DDHe<sup>12</sup>**. We believe that the point **DHo** is very important since according to the Shilnikov criterion [75] the Lorenz attractor originates from this point (see [76] for more details).

The above degeneracies are organized by the codimension-three global bifurcations:

- **DDHe<sup>2</sup>**, degenerate heteroclinic connection because  $\delta_{12} = 1$  and  $E_2$  changes from real saddle to saddle-focus.
- **DDHe<sup>12</sup>**, degenerate heteroclinic connection between  $E_1$  (with  $\delta_1 = 1$ ) and  $E_2$  (which changes from real saddle to saddle-focus). Due to the richness of the bifurcations that appear around it, the theoretical study of this degeneracy should be addressed in the future.

System (2) is a particular unfolding of the Lorenz system in such a way that, when the continuum of equilibria disappears, it exhibits structurally stable bifurcations. Thus, in Sect. 4.2, studying how the bifurcation sets evolve when  $D$  tends to zero, we have been able to explain, in the Lorenz system, the origin of the global connections which are related to a T-point, a codimension-two heteroclinic loop. Concretely, we have shown that the degenerate global connection **DHe<sup>2</sup>** is their main organizing center (see Fig. 12).

It also deserves to be highlighted that, when we introduce the new term  $Dz^2$  in the Lorenz system, one of the two infinite heteroclinic orbits (that connect the origin and one equilibrium on the sphere at infinity, see [14, Theorem 2(b)]) becomes finite.

**Acknowledgements** The authors thank the suggestions and remarks of the reviewers that have contributed to improve the paper.

**Author contributions** All authors contributed equally to the present research work. All authors read and approved the final manuscript.

**Funding** Funding for open access publishing: Universidad de Sevilla/CBUA This work has been partially supported by the *Ministerio de Economía y Competitividad* (MTM2017-87915-C2-1-P), by the *Ministerio de Ciencia, Innovación y Universidades* (PGC2018-096265-B-I00, PID2021-123200NB-I00) and by the *Consejería de Economía, Innovación, Ciencia y Empleo de la Junta de Andalucía* (projects FQM-276, TIC-0130, P20\_01160 and UHU-1260150).

**Data availability** The data that support the findings of this study are available from the corresponding author upon reasonable request. The numerics of the figures were obtained by AUTO/HomCont and Matlab.

### Declarations

**Conflict of interest** The authors declare that there is no conflict of interest regarding the publication of the paper.

**Open Access** This article is licensed under a Creative Commons Attribution 4.0 International License, which permits use, sharing, adaptation, distribution and reproduction in any medium or format, as long as you give appropriate credit to the original author(s) and the source, provide a link to the Creative Commons licence, and indicate if changes were made. The images or other third party material in this article are included in the article's Creative Commons licence, unless indicated otherwise in a credit line to the material. If material is not included in the article's Creative Commons licence and your intended use is not permitted by statutory regulation or exceeds the permitted use, you will need to obtain permission directly from the copyright holder. To view a copy of this licence, visit <http://creativecommons.org/licenses/by/4.0/>.

### References

- Lorenz, E.N.: Deterministic non-periodic flows. *J. Atmospheric. Sci.* **20**, 130–141 (1963)
- Haken, H.: Analogy between higher instabilities in fluids and lasers. *Phys. Lett. A* **53**, 77–78 (1975)
- Knobloch, E.: Chaos in the segmented disc dynamo. *Phys. Lett. A* **82**, 43–440 (1981)
- Gorman, M., Widmann, P.J., Robbins, K.A.: Nonlinear dynamics of a convection loop: a quantitative comparison of experiment with theory. *Physica D* **19**, 255–267 (1986)
- Elgin, J.N., Molina-Garza, J.B.: Traveling wave solutions of the Maxwell–Bloch equations. *Phys. Rev. A* **35**, 3986–3988 (1987)
- Knobloch, E., Proctor, M.R.E., Weiss, N.O.: Heteroclinic bifurcations in a simple model of double-diffusive convection. *J. Fluid Mech.* **239**, 273–292 (1992)
- Poland, D.: Cooperative catalysis and chemical chaos: a chemical model for the Lorenz equations. *Physica D* **65**, 86–99 (1993)
- Cuomo, K.M., Oppenheim, A.V.: Circuit implementation of synchronized chaos with applications to communications. *Phys. Rev. Lett.* **71**, 65–68 (1993)
- Hemati, N.: Strange attractors in brushless DC motors. *IEEE Trans. Circuits-I* **41**, 40–45 (1994)
- Alexeev, I.: Lorenz system in the thermodynamic modelling of Leukaemia malignancy. *Med. Hypotheses* **102**, 150–155 (2017)
- Glendinning, P., Sparrow, C.: T-points: a codimension two heteroclinic bifurcation. *J. Stat. Phys.* **43**, 479–488 (1986)
- Tucker, W.: The Lorenz attractor exists. *C. R. Acad. Sci.* **328**, 1197–1202 (1999)
- Barrio, R., Serrano, S.: Bounds for the chaotic region in the Lorenz model. *Physica D* **238**, 1615–1624 (2009)
- Messias, M.: Dynamics at infinity and the existence of singularly degenerate heteroclinic cycles in the Lorenz system. *J. Phys. A* **42**, 115101 (2009)
- Llibre, J., Messias, M., da Silva, P.R.: Global dynamics of the Lorenz system with invariant algebraic surfaces. *Int. J. Bifurc. Chaos* **20**, 3137–3155 (2010)
- Algaba, A., Fernández-Sánchez, F., Merino, M., Rodríguez-Luis, A.J.: Centers on center manifolds in the Lorenz, Chen and Lü systems. *Commun. Nonlinear Sci. Numer. Simul.* **19**, 772–775 (2014)
- Algaba, A., Fernández-Sánchez, F., Merino, M., Rodríguez-Luis, A.J.: Analysis of the T-point-Hopf bifurcation in the Lorenz system. *Commun. Nonlinear Sci. Numer. Simul.* **22**, 676–691 (2015)
- Creaser, J.L., Krauskopf, B., Osinga, H.M.:  $\alpha$ -flips and T-points in the Lorenz system. *Nonlinearity* **28**, R39–R65 (2015)
- Doedel, E.J., Krauskopf, B., Osinga, H.M.: Global organization of phase space in the transition to chaos in the Lorenz system. *Nonlinearity* **28**, R113–R139 (2015)
- Algaba, A., Gamero, E., Merino, M., Rodríguez-Luis, A.J.: Resonances of periodic orbits in the Lorenz system. *Nonlinear Dyn.* **84**, 2111–2136 (2016)
- Leonov, G.A., Kuznetsov, N.V., Korzhemanova, N.A., Kuzakin, D.V.: Lyapunov dimension formula for the global attractor of the Lorenz system. *Commun. Nonlinear Sci. Numer. Simul.* **41**, 84–103 (2016)
- Algaba, A., Merino, M., Rodríguez-Luis, A.J.: Superluminal periodic orbits in the Lorenz system. *Commun. Nonlinear Sci. Numer. Simul.* **39**, 220–232 (2016)
- Algaba, A., Freire, E., Gamero, E., Rodríguez-Luis, A.J.: Analysis of Hopf and Takens–Bogdanov bifurcations in a modified van der Pol–Duffing oscillator. *Nonlinear Dyn.* **16**, 369–404 (1998)
- Algaba, A., Freire, E., Gamero, E., Rodríguez-Luis, A.J.: A three-parameter study of a degenerate case of the Hopf–Pitchfork bifurcation. *Nonlinearity* **12**, 1177–1206 (1999)
- Algaba, A., Freire, E., Gamero, E., Rodríguez-Luis, A.J.: On a codimension-three unfolding of the interaction of degenerate Hopf and pitchfork bifurcations. *Int. J. Bifurc. Chaos* **9**, 1333–1362 (1999)
- Algaba, A., Freire, E., Gamero, E., Rodríguez-Luis, A.J.: A tame degenerate Hopf-pitchfork bifurcation in a modified van der Pol–Duffing oscillator. *Nonlinear Dyn.* **22**, 249–269 (2000)
- Gamero, E., Freire, E., Rodríguez-Luis, A.J., Ponce, E., Algaba, A.: Hypernormal form calculation for triple-zero

- degeneracies. *Bull. Belgian Math. Soc. Sim.* **6**, 357–368 (1999)
28. Champneys, A.R., Rodríguez-Luis, A.J.: The non-transverse Shil'nikov–Hopf bifurcation: uncoupling of homoclinic orbits and homoclinic tangencies. *Physica D* **128**, 130–158 (1999)
  29. Freire, E., Rodríguez-Luis, A.J., Gamero, E., Ponce, E.: A case study for homoclinic chaos in an autonomous electronic circuit. A trip from Takens–Bogdanov to Hopf–Šil'nikov. *Physica D* **62**, 230–253 (1993)
  30. Gonchenko, S., Kazakov, A., Turaev, D., Shilnikov, A.L.: Leonid Shilnikov and mathematical theory of dynamical chaos. *Chaos* **32**, 010402 (2022)
  31. Champneys, A.R., Kuznetsov, Y.A.: Numerical detection and continuation of codimension-two homoclinic bifurcations. *Int. J. Bifurc. Chaos* **4**, 795–822 (1994)
  32. Homburg, A.J., Sandstede, B.: Homoclinic and heteroclinic bifurcations in vector fields. In: Broer, H., et al. (eds.) *Handbook of Dynamical Systems*, vol. 3, pp. 379–524. Elsevier, Amsterdam (2010)
  33. Guckenheimer, J., Holmes, P.J.: *Nonlinear Oscillations, Dynamical Systems, and Bifurcations of Vector Fields*. Springer, New York (1983)
  34. Wiggins, S.: *Introduction to Applied Dynamical Systems and Chaos*. Springer, New York (2003)
  35. Kuznetsov, Y.A.: *Elements of Applied Bifurcation Theory*. Springer, New York (2004)
  36. Chow, S.N., Li, C., Wang, D.: *Normal Forms and Bifurcation of Planar Vector Fields*. Cambridge University Press, Cambridge (1994)
  37. Khorozov, E.I.: Versal deformations of equivariant vector fields in the case of symmetry of order 2 and 3. *Trans. Petrovski Seminar* **5**, 163–192 (1979). (in Russian)
  38. Carr, J.: *Applications of Center Manifold Theory*. Springer, New York (1981)
  39. Algaba, A., Gamero, E., Rodríguez-Luis, A.J.: A bifurcation analysis of a simple electronic circuit. *Commun. Nonlinear Sci. Numer. Simul.* **10**, 169–178 (2005)
  40. Gazor, M., Moazeni, M.: Parametric normal forms for Bogdanov–Takens singularity; the generalized saddle-node case. *Discrete Contin. Dyn. Syst.* **35**, 205–224 (2015)
  41. Zhan, F., Liu, S., Zhang, X., Wang, J., Lu, B.: Mixed-mode oscillations and bifurcation analysis in a pituitary model. *Nonlinear Dyn.* **94**, 807–826 (2018)
  42. Gazor, M., Sadri, N.: Bifurcation controller designs for the generalized cusp plants of Bogdanov–Takens singularity with an application to ship control. *SIAM J. Control. Optim.* **57**, 2122–2151 (2019)
  43. Durga Prasad, K., Prasad, B.S.R.V.: Qualitative analysis of additional food provided predator–prey system with anti-predator behaviour in prey. *Nonlinear Dyn.* **96**, 1765–1793 (2019)
  44. Algaba, A., Chung, K.W., Qin, B.W., Rodríguez-Luis, A.J.: A nonlinear time transformation method to compute all the coefficients for the homoclinic bifurcation in the quadratic Takens–Bogdanov normal form. *Nonlinear Dyn.* **97**, 979–990 (2019)
  45. Algaba, A., Domínguez-Moreno, M.C., Merino, M., Rodríguez-Luis, A.J.: Double-zero degeneracy and heteroclinic cycles in a perturbation of the Lorenz system. *Commun. Nonlinear Sci. Numer. Simul.* **111**, 106482 (2022)
  46. Maurício de Carvalho, J.P.S., Rodrigues, A.A.: SIR model with vaccination: bifurcation analysis. *Qual. Theory Dyn. Syst.* **22**, 105 (2023)
  47. Wang, Q., Huang, W., Feng, J.: Multiple limit cycles and centers on center manifolds for Lorenz system. *Appl. Math. Comput.* **238**, 281–288 (2014)
  48. Algaba, A., Domínguez-Moreno, M.C., Merino, M., Rodríguez-Luis, A.J.: Study of the Hopf bifurcation in the Lorenz. Chen and Lü systems. *Nonlinear Dyn.* **79**, 885–902 (2015)
  49. Algaba, A., Domínguez-Moreno, M.C., Merino, M., Rodríguez-Luis, A.J.: Takens–Bogdanov bifurcations of equilibria and periodic orbits in the Lorenz system. *Commun. Nonlinear Sci. Numer. Simul.* **30**, 328–343 (2016)
  50. Algaba, A., Domínguez-Moreno, M.C., Merino, M., Rodríguez-Luis, A.J.: A review on some bifurcations in the Lorenz system. In: Carmona, V. et al. (eds) *Nonlinear Systems, Vol. 1. Understanding Complex Systems*, pp. 3–36. Springer, Cham (2018)
  51. de Witte, V., Govaerts, W., Kuznetsov, Y.A., Friedman, M.: Interactive initialization and continuation of homoclinic and heteroclinic orbits in MATLAB, *ACM Trans. Math. Software* **38**, art. no. 18 (2012)
  52. Barrio, R., Shilnikov, A., Shilnikov, L.: Kneadings, symbolic dynamics and painting Lorenz chaos. *Int. J. Bifurcat. Chaos* **22**, 1230016 (2012)
  53. Bykov, V.V.: The generation of periodic motions from the separatrix contour of a three-dimensional system. *Uspekhi Matematicheskikh Nauk* **32**, 213–214 (1977). (in Russian)
  54. Bykov, V.V.: On the generation of a non-trivial hyperbolic set from a contour formed by separatrices of saddles. In: *Methods of the Qualitative Theory of Differential Equations*, pp. 22–32, Gorky University Press, Gorky (1988)
  55. Bykov, V.V.: The bifurcations of separatrix contours and chaos. *Physica D* **62**, 290–299 (1993)
  56. Fernández-Sánchez, F., Freire, E., Rodríguez-Luis, A.J.: T-Points in a  $\mathbb{Z}_2$ -symmetric electronic oscillator. (I) Analysis. *Nonlinear Dyn.* **28**, 53–69 (2002)
  57. Algaba, A., Fernández-Sánchez, F., Merino, M., Rodríguez-Luis, A.J.: Structure of saddle-node and cusp bifurcations of periodic orbits near a non-transversal T-point. *Nonlinear Dyn.* **63**, 455–476 (2011)
  58. Rodrigues, A.A.P.: Repelling dynamics near a Bykov cycle. *J. Dyn. Differ. Equ.* **25**, 605–625 (2013)
  59. Kokubu, H., Roussarie, R.: Existence of a singular degenerate heteroclinic cycle in the Lorenz system and its dynamical consequences: Part I. *J. Dyn. Differ. Equ.* **16**, 513–557 (2004)
  60. Sparrow, C.: *The Lorenz Equation: Bifurcations. Chaos and Strange Attractors*. Springer, New York (1982)
  61. Keener, J.P.: Infinite period bifurcation and global bifurcation branches. *SIAM J. Appl. Math.* **41**, 127–144 (1981)
  62. Qin, B.W., Chung, K.W., Algaba, A., Rodríguez-Luis, A.J.: High-order approximation of heteroclinic bifurcations in truncated 2D-normal forms for the generic cases of Hopf-zero and non-resonant double Hopf singularities. *SIAM J. Appl. Dynam. Syst.* **20**, 403–437 (2021)
  63. Doedel, E.J., Champneys, A.R., Dercole, F., Fairgrieve, T., Kuznetsov, Y., Oldeman, B.E., Paffenroth, R., Sandstede, B., Wang, X., Zhang, C.: Auto07-P: Continuation and bifurca-

- tion software for ordinary differential equations (with HomCont). Technical report, Concordia University (2010)
64. Broer, H., Roussarie, R., Simó, C.: Invariant circles in the Bogdanov–Takens bifurcation for diffeomorphisms. *Ergod. Theor. Dyn. Syst.* **16**, 1147–1172 (1996)
  65. Krauskopf, B., Oldeman, B.E.: Bifurcations of global reinjection orbits near a saddle-node Hopf bifurcation. *Nonlinearity* **19**, 2149–2167 (2006)
  66. Rademacher, J.D.M.: Homoclinic orbits near heteroclinic cycles with one equilibrium and one periodic orbit. *J. Differ. Equ.* **218**, 390–443 (2005)
  67. Glendinning, P.: Bifurcations near homoclinic orbits with symmetry. *Phys. Lett. A* **103**, 163–166 (1984)
  68. Afraimovich, V.S., Bykov, V.V., Shilnikov, L.P.: On the origin and structure of the Lorenz attractor. *Dokl. Akad. Nauk SSSR* **234**, 336–339 (1977). **(in Russian)**
  69. Afraimovich, V.S., Bykov, V.V., Shilnikov, L.P.: Attractive nonrough limit sets of Lorenz-attractor type. *Trudy Moskovskoe Matematicheskoe Obshchestvo* **44**, 150–212 (1982). **(in Russian)**
  70. Hirschberg, P., Knobloch, E.: Sil’nikov-Hopf bifurcation. *Physica D* **62**, 202–216 (1993)
  71. Belyakov, L.A.: Bifurcation set in a system with homoclinic saddle curve. *Math. Notes Acad. Sci. USSR* **28**, 910–916 (1980)
  72. Belyakov, L.A.: Bifurcation of systems with homoclinic curve of a saddle-focus with saddle quantity zero. *Math. Notes Acad. Sci. USSR* **36**, 838–843 (1984)
  73. Kuznetsov, Y.A., de Feo, O., Rinaldi, S.: Belyakov homoclinic bifurcations in a tritrophic food chain model. *SIAM J. Appl. Math.* **62**, 462–487 (2001)
  74. Algaba, A., Merino, M., Rodríguez-Luis, A.J.: Homoclinic connections near a Belyakov point in Chua’s equation. *Int. J. Bifurc. Chaos* **15**, 1239–1252 (2005)
  75. Shilnikov, L.: The bifurcation theory and quasi-hyperbolic attractors. *Uspehi Mat. Nauk* **36**, 240–241 (1981)
  76. Kazakov, A.: On bifurcations of Lorenz attractors in the Lyubimov–Zaks model. *Chaos* **31**, 093118 (2021)

**Publisher’s Note** Springer Nature remains neutral with regard to jurisdictional claims in published maps and institutional affiliations.